Hygrothermal Effects on Fiber Reinforced Polyphenylene Sulphide Composites

Humidity uptake and temperature influence on mechanical properties of glass and carbon fiber reinforced polyphenylene sulphide composites

Delft, September 2011

Author:
Emmanuel Suarez Cabrera

Delft University of Technology

Universidad Carlos III de Madrid

PREFACE

This document is the report on the master thesis project of Emmanuel Suarez Cabrera, student at the Universidad Carlos III de Madrid, Escuela Politecnica Superior. The thesis research was conducted in eleven months as a guest student at the Delft University of Technology, faculty of Aerospace Engineering, conform the five year study curriculum prescribed by the Escuela Politecnica Superior. This report was filed as part of the graduation procedure.

The report can be of use for material engineers conducting research in the field of durability of fibre reinforced thermoplastic composites.

Special thanks go to Ir. Julie Teuwen, my supervisor, for her support, comments and for keeping me focused during my research, as well as to D. Ir. Irene Fernandez Villegas and Ir. Paola Carnevale for their help, and to D. Ir. Jose Manuel Torralba for giving me the chance to apply for a guest student position at Aerospace Faculty of TU Delft.

SUMMARY

In the ever-continuing quest for greener and cheaper aerospace materials, the Durability Group, part of the Design and Production of Composite Structures Department at the faculty of Aerospace Engineering of the Delft University of Technology is focusing on the use of new thermoplastic composites for aerospace structures. Currently the introduction of Nylon composites in the aerospace industry is being investigated. Nylon as a thermoplastic matrix for fibre reinforced composites can be bought at competitive prices but a lot of factors can influence the mechanical and dimensional stability of Nylon over time. Hygrothermal effects in fiber reinforced composite researches have to be undertaken in order to achieve better understanding of the thermoplastic durability.

This research will focus on the characterisation of carbon and glass fibre reinforced polyphenylene sulphide (CF/ PPS and GF/PPS) composite hygrothermal behaviour, as it is one of the most common used material in the aerospace industry. The goals of this work are to determine the water absorption in reinforced PPS composites as a function of time in hot-wet environment and to study the effect of temperature and humidity on mechanical properties. The know-how and information obtained about reinforced PPS composites could be used in the future for comparison with new material, as Nylon, which could replace PPS in the aerospace industry. More knowledge about the differences between glass and carbon fiber reinforcement is found.

The two materials (PPS/CF and PPS/GF) were produced by hand film stacking technique and hot pressing. Ultrasonic C-scan, a non-destructive inspection technique, was used subsequently to analyse the quality of the panels. Later specimens of the composites were dried and conditioned for periods of one month and two months in a climate chamber. Mechanical testing, including tensile, in plane shear and three point bending, was performed on dry material, one month and two month conditioned material . Tensile testing was performed at three different temperatures. A gravimetric method was used to derive the diffusion coefficient of the materials, assuming Fickian diffusion model, as well as to measure the saturation moisture absorption, in a temperature and humidity controlled environment. Diffusion coefficients were calculated, and the measured saturation moisture absorptions were compared to the estimated ones assisted by MATLAB software curve fitting tool. A scanning electron microscope (SEM) was used to take micrographs of non tested and tested material, dry and saturated specimens, combined with Energy Dispersive X-Ray Spectroscopy (EDS) to check present phases and their contents.

This research concluded that PPS composites absorb low levels of humidity; 0.17% for CF/PPS and 0.21% for GF/PPS at 80ºC and 90%RH after 2 months of conditioning. The diffusion of the water in the composite can be modelled assuming Fick's diffusion law. Diffusion coefficients of 0.005 and 0.010 mm^2/h were derived for CF/PPS and for GF/PPS respectively. A rather high variation coefficient, 35% and 37%, was found though. Some recommendations that could be followed to improve the repeatability of the diffusion coefficients are suggested below:

1. Bigger specimens or sealed edge specimens shall be used to follow procedure A of the ASTM D5229, especially in very low humidity uptake saturation levels, like those found in this research.
2. As many weightings as possible in the first 72 hours of conditioning are needed for the linear part of the Fick's law. This part of the model can extend to this short initial period.
3. A weighing method error of ±10 mg is recommended to be used to round off weights of specimens.

CF/PPS presented a significant retention of mechanical properties even after saturation and at tensile testing temperatures above Tg (120°C). GF/PPS was sensitive to humidity uptake when tested under matrix and interface dominant tests like in-plane shear and three point bending. Losses up to 30% of mechanical properties were calculated after saturation in the mentioned tests.

SEM/EDS technique came up to be useful to find humidity uptake in the case of CF/PPS since no oxygen is present in the dry system. On the other hand, the presence of oxygen in the oxides of the GF made this technique non-applicable in this case. An accidental contamination of Aluminium in the climate chamber arose as a possible method for tracing in future humidity uptake researches. Different cations were found when analysing GF, part of them belonging to the fiber itself, and the rest to the sizing assisted by EDS technique. The polar nature of these elements is assigned as one of the reason of the sensitivity of the glass fiber system to humidity uptake. The coupling of these elements with water seems to explain the weakening of the interface.

This hypothesis was supported by the micrographs that showed a detachment of the GF and the matrix in saturated tested specimens. The roughness of the CF versus the smoothness of the GF could also explain the more difference in interface behaviour.

The influence of testing temperature, where a decrease in properties was found both for CF/PPS and GF/PPS, is explained by the presence of a glass transition temperature (Tg) of thermoplastics. The softening of the matrix above Tg could explain the decrease in tensile properties. Matrix dominant tests should be performed to show this effect even more.

While the effect of temperature damage can be observed almost instantaneously, a similar loss in properties was observed after humidity uptake after 2 months.

LIST OF CONTENTS

CHAPTER 1: INTRODUCTION

The department of Design and Production of Composite Structures (DPCS) within the Faculty of Aerospace Engineering at the Delft Technology University is focused on composite materials as they come up as a solution for the industry demands of lighter, cheaper, and more durable and sustainable components. At the same time composites, if properly used, allow a broad variety of final forms and high performance behaviour. The development of new designs, manufacturing and materials constitute the DPCS aim, and their integration, its philosophy.

In the search of new materials, material performance knowledge is essential to better understand material properties and the behaviour in use, affected by environmental conditions as humidity or temperature. Design and manufacturing should take in account those effects. Moreover, nowadays the concept of life cycle of the component is integrated in the design, and it is mandatory to improve and develop durability investigations. This is the task of the Durability group, within the DPCS.

One of the external projects of this group is The "Clean Sky" Joint Technology Initiative (JTI). The durability group collaborates with the "Eco-Design" technology platform within the JTI. In this platform, Nylon, an engineering polymer, is being studied as a replacement of high performance thermoplastic matrix, as polyphenylene sulfide (PPS), in composites, due to its lower cost of processing and better recyclability. In the case of Nylon, dimensional stability and mechanical response depend on the hygrothermal conditions. Further research on this influence is needed. Some relations between these polymers are shown in the well known "Polymer Pyramid" in the Fig.1.1 (Ref. 1.1).

Studying on PPS, commonly used in aerospace industry, is a good starting point to establish the range of different physical and mechanical parameters and its variability with hygrothermal effects. The goals of this research are to evaluate the moisture absorption in the PPS reinforced with carbon and glass fibers (CF and GF) under a certain condition of temperature and humidity, to test mechanical properties of the dried and conditioned material, at different temperatures in the case of tensile tests, and to find out the relation between the microstructure before and after the humidity uptake, and the influence of temperature, in order to better understand the hygrothermal effects on the material behaviour.

The structure of this report goes through the existing literature about hygrothermal effects on composites, the application of fickian law to characterize diffusion, focusing later on PPS, CF and GF in Chapter 2. The research questions are formulated in Chapter 3. How manufacturing, quality control, obtaining specimens, conditioning, mechanical testing and SEM/EDS analysis were undertaken is explained in Chapter 4. Chapter 5 show the results found and finally in Chapter 6, conclusions and recommendations are presented.

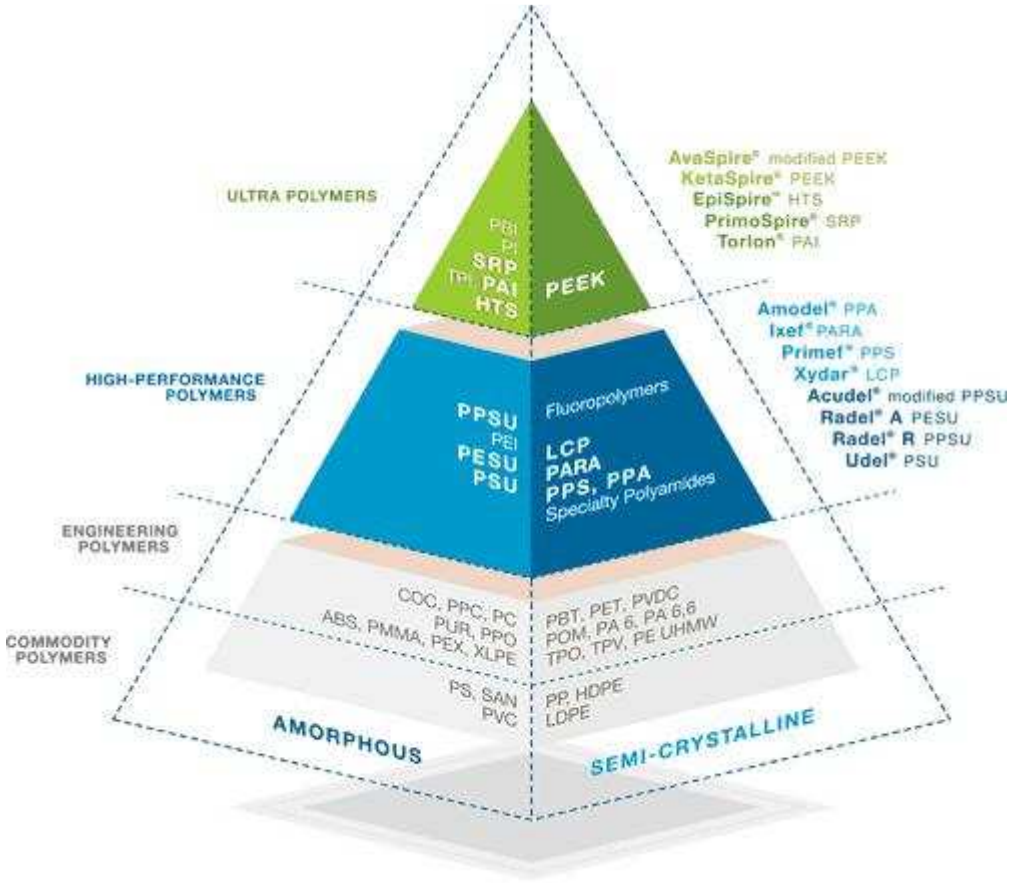

Fig.1.1 "The Polymer Pyramid" (Ref. 1.1).

CHAPTER 2: HYGROTHERMAL EFFECTS IN FIBER REINFORCED COMPOSITES

In this chapter, the ageing of composites, a classification for it, the effect of temperature and humidity and a review in the particular case of PPS are described. Also the fiber manufacturing, focusing on the surface treatment which determine the interface between resin and fiber and its behaviour, in the cases of CF and GF are explained as essential concerns when researching on the hygrothermal effects on the composite behaviour.

2.1 Introduction to composites

The three basic components of advanced polymer matrix composites (PMC) are matrix, fiber and interface. Interesting properties are given by the polymeric matrix as easy processing, low cost and corrosion resistance, meanwhile in many circumstances the polymer is the main responsible for degradation or dimensional changes. Applications with loads or environments that affects the matrix, make the visco-elastic nature of the matrix becomes the dominant factor. This behaviour is known as ageing of the composite.

2.2 Ageing

The process of change in properties over time in PMC is loosely referred to as ‘ageing’. Ageing may be broadly categorized by three primary mechanisms: chemical, physical and mechanical. The interaction (if any) between these three areas is highly dependent on two variables: material characteristics (matrix, fiber and interface) and ageing environment (Ref.2.1 p.3).

Three important terms in PMC´s ageing which have to be described are (Ref.2.1 p.4):

1. The environmental degradation factor is the general term for specific use environmental conditions. Temperature, moisture, mechanical load and ultraviolet radiation are all environmental degradation factors.
2. The critical degradation mechanism refers to the fact that polymer materials are susceptible to attack by a specific set of environmental degradation factors which includes influences due to chemical, physical and mechanical processes. The critical degradation mechanism is the mechanism that occurs due to this attack and results in a significant change in one or more bulk physical properties of the material system.
3. Accelerated ageing is defined as the process or processes required to accelerate a specific critical degradation mechanism or mechanisms relative to a baseline ageing condition; thereby resulting in the material reaching the same aged end-state as a real-time aged material, but in less time.

Although knowledge on long-term behaviour is required to asses the durability of a material completely, the accelerated ageing is interesting not only in terms of cost reduction of the testing procedure but also to characterize which materials would be rejected before going for more long- lasting tests or suggest improvements in the material processing.

2.2.1. Chemical ageing

Chemical ageing is related to irreversible changes in the polymer chain or network through mechanisms such as cross-linking or chain scission. Chemical degradation mechanisms include thermo-oxidative, thermal and hydrolytic ageing. At typical PMC operation temperatures, cross-linking and oxidation are the dominant chemical ageing mechanisms. Thermo-oxidative degradation becomes more important with longer exposure times and higher temperatures. Frequently, chemical ageing results in an increase in cross-linking density that can lead to changes in material densification and increases the glass transition temperature (Tg) (Ref. 2.1 p.5)

2.2.2 Physical ageing

Physical ageing will occur when a polymer is cooled rapidly below its Tg and the material evolves gradually towards thermodynamic equilibrium, meanwhile this evolution happens instantaneously for T>Tg. Physical ageing occurs after processing inherently. This evolution is characterized by changes in the free volume, enthalpy and entropy which have an effect on the mechanical properties. Physical ageing is responsible for changes over time of modulus, strength and ductility for polymers in the glassy region, where most of polymer composites structures are used. Physical ageing is more important on long-term durability and is influenced strongly by mean temperature and the thermal history. Physical ageing changes are reversible in the case of amorphous polymers, by heating at T>Tg and subsequently quenching rapidly (Ref.2.1 pp.5-6).

2.2.3 Mechanical ageing

Mechanical ageing happens under load states that produce irreversible changes. These changes are observable on the macroscopic scale. This type of degradation includes matrix cracking, delamination, interface degradation, fiber breaks, and inelastic deformation. The reached plastic strains are defined as time-independent but time-dependent strains can also be observed often in plastic composites. Creep is the continuous time-dependent deformation of a material under constant stress (Ref. 2.1 pp.6-7).

2.3 Temperature

Temperature has a big influence in PMCs. Particularly semi-crystalline thermoplastics (e.g. PEEK, PPS or Nylon) have a second-order transition temperature below the melting temperature (Tm) called the glass transition (Tg), associated with the conversion from glassy to rubbery state of the amorphous regions. The Tm, a first-order transition temperature, is linked to the change from solid to liquid state of the glass phase of the polymer. Fig.2.1 (Ref.2.2) depicts the change of the Young's modulus of two theoretical polymers, one semi-crystalline and the other amorphous, assuming both of them have the same Tg and Tm. The temperature effect on composite loss of properties can be considered a type of chemical ageing.

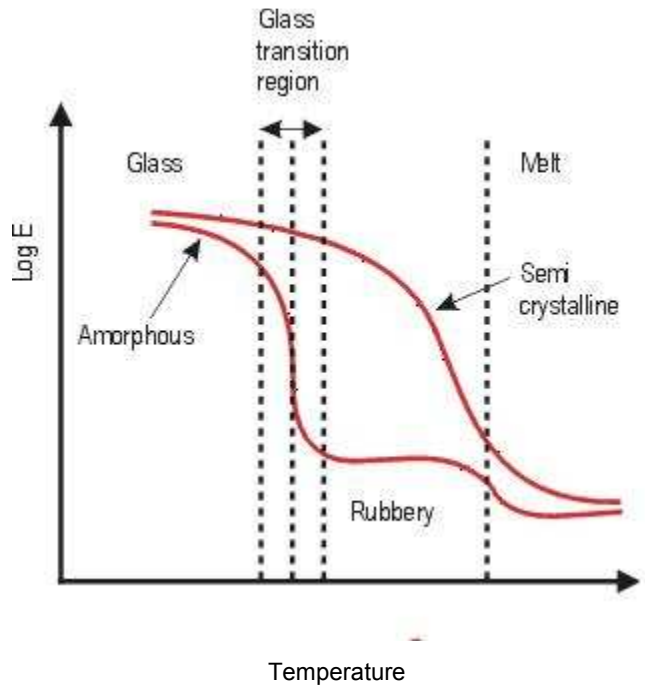

Fig. 2.1 The effect of temperature on the Elastic Modulus (assuming both types of polymer have the same Tg and Tm (Ref.2.2).

Aerospace traditionally relied on expensive high performance materials (e.g. high Tg thermoplastics, thermosets with continuous fibers). In the drive for more recyclable and less expensive fabrication techniques, materials with lower Tg are desirable. Table 2.1 shows the comparison of Tg and Tm for an ultra polymer (PEEK), a high performance polymer (PPS) and a engineering polymer (Nylon 6). This table illustrates the tendency of the composite industry mentioned above (Ref. 2.2). A compromise solution has to be found between the temperature working conditions usually below Tg and the use of materials with lower Tg, due to the loss of properties observed above Tg.

Table 2.1 Tg and Tm of PEEK, PPS and PA6 (Ref. 2.2).

Polymer	**Tg (°C)**	**Tm (°C)**
Polyetheretherketone (PEEK)	145	335
Polyphenylene sulphide (PPS)	90	285
Nylon 6 (PA6)	50	215

2.4 Humidity

The presence of humidity leads to hydrolytic degradation, due to the diffusion of water into the matrix and the subsequent plasticization of the matrix, through the fiber-matrix interface or through cracks and voids in the composite. This is true for inorganic fiber composites such as boron, graphite or glass where the fibers do not seem to absorb moisture. For organic fiber composites, diffusion in the filament may be considered as the forth mechanism of moisture absorption (Ref. 2.3 pp.2-3). Hydrolytic degradation is a type of chemical ageing.

Mechanical properties are sensitive to this humidity uptake. For example, a decrease in fracture toughness has been observed when a polymeric composite was simultaneously exposed to water and mechanical stress. (Han and Nairm, 2003). Viscoelastic properties such as creep may also be susceptible to moisture-induced degradation.

The diffusivity of a polymeric composite is a function of specimen geometry, moisture concentration, temperature, and time and is often modelled using the standard Fick´s law as described in Springer(1981) (Ref. 2.1 pp.26-27).

Considering a thin plate of composite laminate as shown in Fig.2.2 (Ref.2.4), the diffusion can be described by a Fickian diffusion model. Since temperature reaches equilibrium about ten times faster than the moisture concentration does, the temperature inside the material can be considered as the outside temperature.

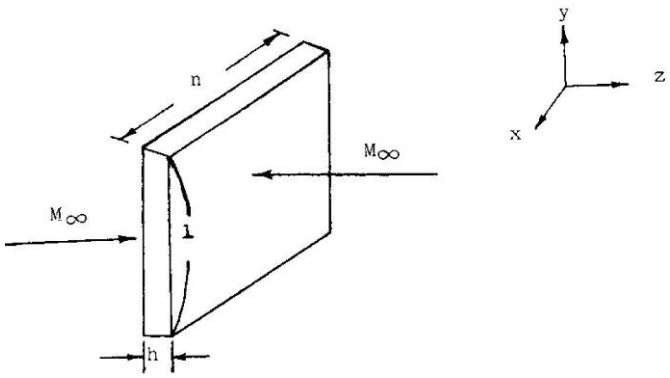

Fig. 2.2 A thin laminate ((h/l)<<1, (h/n)<<1) immersed in water (Ref. 2.4).

For a Fickian diffusion (Ref.2.5 p.10):

$$\frac{\partial c}{\partial t} = D_z \frac{\partial^2 c}{\partial z^2}$$

c – concentration of moisture $\left[\text{g/mm}^3\right]$

t – time $\left[\text{s}\right]$

D_z – Fickian material difussion constant through-the-thickness $\left[\text{mm}^2/\text{s}\right]$

z – through-the-thickness direction $\left[\text{mm}\right]$(see fig. 2.2)

Eq.2.1

The boundary and initial conditions are:

$$c = c_i \; at \; 0 < z < h \;\; t \le 0$$

$$c = c_\infty \; at \; z = 0; z = h \;\; t > 0$$

c_i – specimen moisture concentration at t=0 $\left[\text{g/mm}^3\right]$

c_∞ – specimen moisture concentration at equilibrium $\left[\text{g/mm}^3\right]$

h – thichness $\left[\text{mm}\right]$

Thus the solution of Eq.2.1 can be derived as (Ref. 2.4):

$$\frac{c - c_i}{c_\infty - c_i} = 1 - \frac{4}{\pi} \sum_{i=1}^{\infty} \frac{1}{(2i+1)} \sin\left[\frac{(2i+1)z\pi}{h}\right] \exp\left[\frac{-(2i+1)^2 \pi^2 D_z t}{h^2}\right]$$

Eq.2.2

The moisture absorption in the composite, M, is defined as follows:

$$M = \frac{Weight\ of\ wet\ material - weight\ of\ dry\ material}{weight\ of\ dry\ material} \times 100\%$$

Eq.2.3

The moisture absorption can be calculated with the integral (Ref 2.3):

$$M = \int_0^h c(z,t)dz$$

Eq.2.4

At time t, this relationship reduces to (Ref. 2.4):

$$\frac{M - M_i}{M_\infty - M_i} = 1 - \frac{8}{\pi^2} \exp\left(-\frac{\pi^2 D_z t}{h^2}\right)$$

Eq.2.5

At initial time, water absorbed is given by:

$$\frac{M - M_i}{M_\infty - M_i} = 4\left(\frac{D_z t}{h^2 \pi}\right)^{1/2}$$

Eq.2.6

By plotting M versus t one can obtain Fig.2.3 (Ref.2.4). The diffusion coefficient can be derived from the initial slope.

$$D_z = \frac{\pi}{16}\left(\frac{M_2 - M_1}{M_\infty - M_i}\right)^2 \left(\frac{h}{\sqrt{t_2} - \sqrt{t_1}}\right)^2$$

Eq.2.7

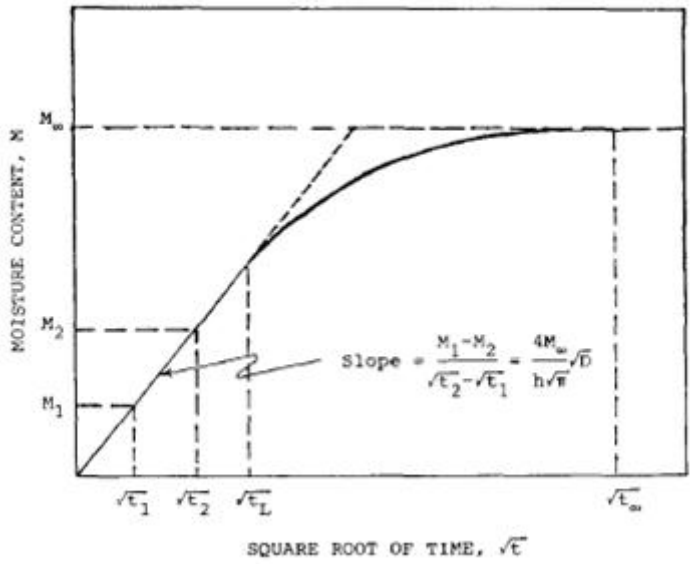

Fig.2.3 Fickian diffusion curve (Ref.2.4).

D is a function of temperature as follows (Ref. 2.3):

$$D_z = D_0 \exp\left(-\frac{E_d}{RT}\right)$$

D_0 – permeability index $\left[\text{mm}^2/\text{s}\right]$

E_d – energy of activation for difussion $\left[\text{J/mol}\right]$

R – universal gas constant $\left[\text{J/(mol}\times\text{K)}\right]$

T – temperature $\left[\text{K}\right]$

Eq.2.8

From the plot of *Ln* (D_2) versus *1/T*, the permeability index, D_0, and activation energy of diffusion, E_d, can be deduced (Ref.2.4).

The moisture concentration may reach a plateau level but plasticization in a polymer may increase over time. For an inhomogeneous material, the presence of water in the material can vary from one region to the next. This non-uniform concentration can impose stresses on the material. In a composite material under constant temperature, this stress can give rise to internal damage in the form of matrix cracks. With internal stresses, micro-cracks that form allow new pathways for moisture uptake or fiber-matrix debonding (Ref. 2.1 p.27).

It was found that interlaminar fracture mechanisms in thermoplastics matrix composites are associated with extensive matrix deformation around the crack tip. A stretching and cavitation process proceeds in the crack tip plastic zone. The extent of matrix deformation depends on the velocity of crack propagation. To increase delamination fracture toughness, both an improved interface and higher matrix toughness were found to be required.

In unidirectional laminates crack propagates between the plies along the fiber direction. In multidirectional laminates, the crack may have a tendency to branch trough the neighbouring plies. Severe edge effects may also occur for multidirectional laminates. (Ref.2.3 pp.8-9).

2.5 Hygrothermal effects in reinforced PPS composites

PPS is an engineering thermoplastic consisting of a polymer backbone that contains disubstituted aromatic rings and divalent sulphur atoms. The polymer is produced by the reaction of para-dichlorobenzene and sodium sulphide in a polar solvent, such as *N*-methylpyrrolidone (NMP), at an elevated temperature according to the following reaction (Ref.2.6):

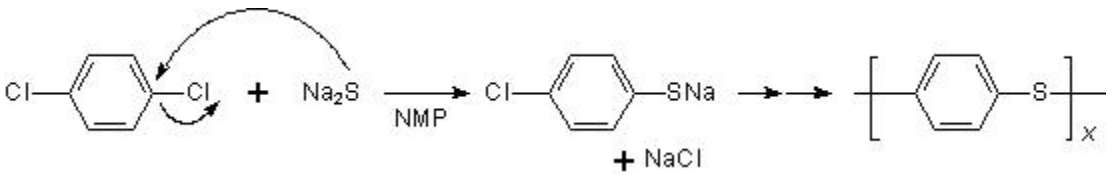

Fig.2.4 Para-dichlorobenzene reacts with Na_2S in NMP at high temperature to produce a simple polymer, PPS (Ref. 2.6).

The uncluttered aromatic ring and simple sulphur bonds are remarkably stable. Therefore, PPS exhibits outstanding high temperature stability, inherent flame resistance, and good chemical resistance. It is essentially insoluble, in fact, no chemical has been found to dissolve it readily below 200°C. Relatively few materials react chemically with PPS even at high temperatures. Its structure promotes a high degree of crystallinity.

The PPS used as the polymer matrix for high performance composites is a modified polymer in which the polymerization reaction is carried out directly to a high molecular weight. This result in a tough PPS polymer which can be used for injection moulding compounds, long fiber reinforced composites, such as random fiber stampable sheets, continuous fiber fabric prepregs, and unidirectional fiber prepregs tapes.

PPS is a semi-crystalline polymer with excellent thermal and mechanical properties. It has found widespread use in the electrical, electronic, transportation, appliance and coatings industries.

The full potential of fiber reinforcement is achieved thanks to a higher molecular weight version of the polymer, with long well impregnated fiber reinforcement of carbon, aramid or glass fibers.

In summary, PPS composites have:

- High strength
- High stiffness
- Good impact toughness
- High temperature resistance
- Excellent solvent resistance
- Excellent corrosion resistance
- Thermal stability
- Low moisture absorption
- Ease of processing
- Easily controllable, predictable crystallinity
- Faster fabrication rates
- Reduced handling and storage problems
- Improved reparability characteristics
- Capability of fusion bonding
- Short cycle time for moulding
- Low smoke generation and flame resistant
- Ability to reuse scraps

(Ref.2.7 pp. 1-4)

2.5.1 Water absorption in PPS

Works by Chen-Chi et al. (Ref.2.4) on CF/PPS composites showed that the higher the temperature of conditioning below Tg, the higher the saturation humidity content gets to. Also, for higher values of relative humidity (RH), higher levels of humidity saturation content were found.

The water absorption of CF/PPS is very low, 0.130% wt for an environment of 80°C and 85%RH. The water diffusion behaviour of CF/PPS can be described by Fick's law (Ref.2.4). The diffusion coefficients of CF/PPS for different temperatures are listed in Table 2.2 (Ref.2.4).

Table 2.2 Diffusion Coefficient of water, D, in CF/PPS at various temperatures and 75% RH (Ref.2.4).

PPS/CF	Diffusivity x $10^9 cm^2/s$		
	60°C	70°C	80°C
	35.8	36	37.9

Annealing the composite at 204°C for 2 hours decreased significantly the saturation humidity uptake (from 0.13% to 0.09% for the same conditions of temperature and relative humidity).
From the research by Jirui Chen (1990), at temperatures above the Tg, the humidity saturation found in the composite was less than those found at temperature found below Tg under the same relative humidity (Ref. 2.7 p.43). This can be explained due to the reduction of free volume through the relaxation of residual stresses and the gain of regularity of the crystal part, after exposing the composite to temperatures above the Tg, which reduces the water saturation level.
At the same time this better arrangement can explain the non-expected result by Chen-chi et al. where it is found that the Tg increases with the humidity uptake in environments of 60°C, 80°C, and is accelerated drastically at 95°C, with 75% RH in the three cases. At 95°C Tg reached 125°C after 2000 hours (83 days).
The expected result that has to be kept in reader's mind is explained bv Jirui Chen (1990). Moisture and heat promote the ability of polymers to dilatate. Moisture may infuse into the polymers, separating the polymer molecules, thus reducing their secondary bond attraction, thereby making it easier for the molecules to move past the critical strain levels. This process is a form of plasticization. Heat creates a similar effect. A higher temperature, especially approaching the Tg, causes the materials to expand, thus creating more free volume. Then it is concluded that the PPS matrix is brittle at low temperature and low moisture content. However, when the moisture content and temperature are high, the material exhibits plastic deformation. High moisture content and high temperature soften the PPS matrix and even causes fiber bridging (Ref. 2.7 pp. 53-54).

In Jirui Chen's work is found that GF/PPS fabric reinforced composites, with higher percentages of GF, present higher humidity uptake level. This fact is explained due to two factors: the larger amount of GF, and the lower degree of crystallinity.

2.5.2 Effect of environment on the PPS composite mechanical properties

Tensile tests are one of the commonly-used methods (even though it might not be the best one) to study the environmental effects on the mechanical properties of a composite material.

In tensile tests of CF/PPS at higher temperatures of conditioning, below the Tg, and longer times of exposure, the tensile strength decreases to a constant value for each case. The higher the temperature of conditioning, the higher the decreasing becomes. Conditioning above the Tg, accelerates this trend (Ref 2.4 pp.36-39). In the case of glass fiber reinforced PPS, Jirui Chen (1990) found that the larger the content of moisture is, the more the reduction in tensile strength will be. Even if the resin itself is hygrothermally stable, the moisture penetrates the materials by a wicking action and attacks the glass-resin interfaces, causing delamination or debonding (Ref. 2.7 p.72-73).

The resistance of PPS composites in harsh environments has been studied by Vives et al. (1983). The thermoplastic composite shows good resistance to many chemicals, although the resistance of GF/PPS to the exposure to water is low. At 95°C, a 40% GF/PPS shows a reduction of more than 30% in flexural strength after a five-week exposure period. The same PPS material but unreinforced shows no change in flexural strength with exposure to water (Ref. 2.7 p.10).

Chen-Chi et al. (1991) found in the case of CF/PPS composite that flexural strength decreased with the immersion time, after which it reached a constant value. Also at higher temperature of conditioning at the same relative humidity, flexural strength increased.

The falling weight impact strength decreases with the immersion time, but after certain time it increased. At higher temperatures of conditioning, the falling weight impact decreases, and the recovery of it after time is higher. At a temperature of 95 °C, above the Tg, this trend is accelerated and can be observed for shorter times of exposure. Chen-Chi et al. explained this effect stating that the water diffuses into the interface between the fiber and matrix first, causing stress concentrations and damage to the material. The higher the temperature, the more the water diffuses in, and the lower the impact strength of composite will be at the beginning. However, the impact strength will be increased owing to the molecule rearrangement for a long-time thermal energy supplied. The higher the temperature, the faster the recovery of impact strength happens (Ref 2.4 pp.36-39).

2.6 Carbon fibers

Although CF are broadly used, it is hard to know about how it is made. CF producers are tight-lipped about how their product is manufactured. Each producer's fiber differs from those of its competitors, and the processing details that give each brand its signature characteristics are considered to be intellectual property. Moreover the CF manufacturing process also is notoriously difficult and expensive. The current cadre of CF producers numbers less than a dozen worldwide. These facts explain the veil of secrecy around the manufacturing of CF (Ref.2.8).

CF producers make products that are similar but not identical. CF varies in tensile modulus (or stiffness) and tensile, compressive and fatigue strength. CF, which is available in bundles called tow, comes in many sizes, ranging from 1K to 350K (1K equals 1,000 filaments that range from 5 to 10 μm in diameter). Products also vary in the degree of carbon content and type of surface treatment/coating (Ref.2.8).

In simplest terms, CF is produced by pyrolysis of an organic precursor fiber in an inert atmosphere at temperatures above 982°C. CF manufacture, however, is a complex undertaking. The primary production phases are polymerization and spinning, oxidation (also referred to as stabilization), carbonization, surface treatment and sizing application (Ref.2.8).

Focusing on the goal of this research, the most important phase of manufacturing is the surface treatment and sizing, since the water absorption in the case of inorganic fibers only occurs through the matrix, the interface matrix-resin or cracks and voids as explained above based on the research by Komorowski (1993). Moreover manufacturers state that surface treatment and sizing step is critical to fiber performance and, apart from the precursor, it most differentiates one supplier's product from its competitors' product (Ref.2.8).

During the manufacture of CF, surface treatment is performed to enhance adhesion between matrix resin and CF. Producers use different treatments, but a common method involves pulling the fiber through an electrochemical or electrolytic bath that contains solutions, such as sodium hypochlorite or nitric acid. These materials etch or roughen the surface of each filament, which increases the surface area available for interfacial fiber/matrix bonding and adds reactive chemical groups, such as carboxylic acids (Ref.2.8).

Next, a highly proprietary coating, the sizing, is applied. At 0.5% to 5% of the weight of the CF, sizing protects the CF during handling and processing (e.g., weaving) into intermediate forms, such as dry fabric and prepreg. Sizing also holds filaments together in individual tows to reduce fuzz, improve processability and increase interfacial shear strength between the fiber and matrix resin. CF producers increasingly use a sizing appropriate to the customer's end use, as well as to the specific properties desired in the composite. Polymeric film formers are used, made by the dispersion of particles suspended in water provide a stable chemistry that creates a good coating on the CF when dried (Ref.2.8).

Surface treatment and sizing increase the fiber's total surface area and porosity and alter its surface energy to improve adhesion between the fiber and the resin matrix in a composite, see Fig.2.5 (Ref.2.8).

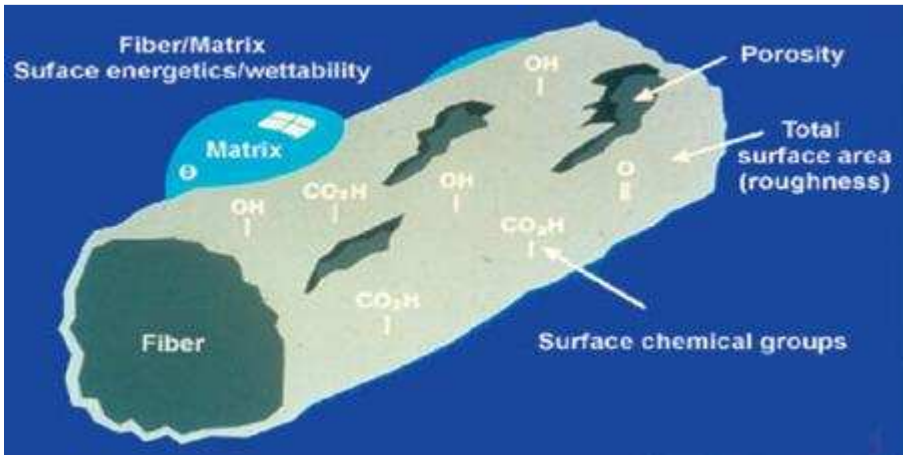

Fig.2.5 Surface characteristics after surface treatment and sizing of fibers (Ref.2.8).

2.7 Glass fibers

GF are made from silica (SiO_2) sand, which melts at 1720°C. If SiO_2 is heated above 1200°C/2192°F then cooled ambiently, it crystallizes and becomes quartz. Glass is produced by altering the temperature and cooldown rates. If pure SiO_2 is heated to 1720°C then cooled quickly, crystallization can be prevented and the process yields the amorphous or randomly ordered atomic structure we know as glass. Although continuously refined and improved, today's GF manufacturers combine this high heat/quick cool strategy with other steps. This process can be broken down into five basic steps: batching, melting, fiberization, coating and drying/packaging (Ref.2.9).

In the batching other ingredients are added to SiO_2 to reduce the working temperature and impart other properties that are useful in specific applications. For example, E-GF, originally aimed at electrical applications, with a composition including SiO_2, Al_2O_3, CaO and MgO, was developed as a more alkali-resistant alternative to the original soda lime glass. S-GF, developed for higher strength, are based on a SiO_2-Al_2O_3-MgO formulation but contain higher percentages of SiO_2 for applications in which tensile strength is the most important property. In Table 2.3 some compositions by weight of selected GF are shown (Ref.2.9).

Apart from the batching that determines the composition of the glass fibers, the coating or sizing is again the critical step that influences on the performance of the interface of the fiber.

Sizing is typically added at 0.5% to 2.0% of the weight of the GF and may include lubricants, binders and/or coupling agents. Again as in the case of CF, the lubricants help to protect the filaments from abrading and breaking as they are collected and wound into forming packages and, later, when they are processed by weavers or other converters into fabrics or other reinforcement forms. Coupling agents cause the fiber to have an affinity for a particular resin chemistry, improving resin wet-out and strengthening the adhesive bond at the fiber-matrix interface. Sizing chemistry is crucial to GF performance (Ref.2.9).

Table 2.3 Compositions by weight of some selected GF (Ref.2.9).

	E-glass w/Boron	E-glass w/o Boron	ECR-glass	S-2 glass	R-glass	Quartz
SiO_2	52-56%	59%	54-62%	64-66%	60-65%	99.9999%
Al_2O_3	12-16%	12.1-13.2%	9-15%	24-26%	17-24%	-
B_2O_3	5-10%	-	-	-	-	-
CaO	16-25%	22-23%	17-25%	-	5-11%	-
MgO	0-5%	3.1-3.4%	0-5%	8-12%	6-12%	-
ZnO	-	-	2.9%	-	-	-
Na_2O	0-1%	0.6-0.9%	1.0%	0-0.1%	0-2%	-
K_2O	trace	0-0.2%	0.2%	-	0-2%	-
TiO_2	0.2-0.5%	0.5-1.5%	2.5%	-	-	-
Zr_2O_3	-	-	-	0-1%	-	-
Li_2O	-	-	-	-	-	-
Fe_2O_3	0.2-0.4%	0.2%	0.1%	0-0.1%	-	-
F_2	0.2-0.7%	0-0.1%	trace	-	-	-

In the case of GF, the coupling agent, almost always an alkoxysilane compound, serves primarily to bond the fiber to the matrix resin. Silanes offer just what is needed to bond two highly dissimilar materials — the GF, which is hydrophilic (bonds easily to water), bonds to a resin that is hydrophobic (insoluble in water and does not bond well to it). Silanes have a silicon end that bonds well to glass, and an opposing organic end that bonds well to resins (Ref.2.10).

CHAPTER 3: RESEARCH QUESTIONS

In this research humidity and temperature were studied as environmental degradation factors. One of the goals is to establish the critical degradation mechanism and the characterization of such mechanism in CF and GF reinforced PPS composites.

The accelerated ageing method was exposure of coupons to a high relative humidity level (90%) and a high temperature (80°C) close to the Tg of PPS (90°C, Ref .3.1) in a climate chamber.
In order to check the effect of the accelerated ageing process mechanical properties (tensile, in-plane shear and bending properties), damage mechanisms (fracture mechanism) and the evaluation of physical parameters (Fick´s diffusion coefficient and content of water after saturation) were evaluated in order to better understand the hydrolytic degradation below Tg.
With tensile tests performed under high temperature below and above Tg, the thermal degradation was screened.

SEM/EDS technique was used to check the changes on microlevel produced by the hygrothermal degradation, as well as to assist to find out the critical degradation mechanism.

CHAPTER 4: EXPERIMENTAL

In this chapter, the way the research was performed will be explained. First of all, the materials used and the manufacturing of the plates will be described after which the quality control of the plates will be discussed. After that, cutting and conditioning of the coupons, the fitting of humidity absorption curve and the mechanical tests will be described and finally the microscopic analysis of cross-sections of the coupons will be discussed.

4.1 Materials

Semi-impregnated (semipreg) CF and GF reinforced PPS rolls were supplied by Tencate Advanced Composites BV Nijverdal, The Netherlands. In Table 4.1 the labelling of the rolls are shown. The woven fabrics had both [0,90]º fiber orientation.

Table 4.1 Roll labelling.

Semi-preg. CF/PPS		Semi-preg. GF/PPS	
Fabric style	CD 0286 050 000	Fabric style	SS 0303 050 020
Finish	8538 43000	Finish	8538 34000
Production order	30071193	Production order	20080717
Roll number	08	Roll number	16
Roll length	30	Roll length	97
Production date	No data	Production date	03. July. 2008

Technical data and extra information about Cetex PPS, the commercial name of these pre-pregs are given by Tencate in Ref.3.1.

4.2 Manufacturing

The rolls of semipreg were unrolled on a cutting table equipped with a computer assisted design (CAD) and computer assisted manufacturing (CAM) cutting machine (Gerber DSC 2500), as shown in Fig.4.1.

The fabrics were cut into 8 squares (580x580) mm^2. Every square was marked to follow the warp direction. In order to compensate the enrolled shape, alternative squares were turned upside down and stacked onto the previous. In this way, a balanced and symmetric laminate was obtained. An 8 layer laminate was formed up by hand-stacking. The minimum number of layers used for in-plane shear is 8 layers (Ref.4.1), as will be discussed in Appendix 4. Moreover, a minimum thickness is needed in order to have quicker moisture absorption through the thickness. The layers were ultrasonic welded in several points two by two with an ultrasonic welder RL35 (Fig.4.2), produced by Rinco Ultrasonic, and then sealed with aluminium tape to consolidate the laminate.

Fig.4.1 Gerber cutting machine.

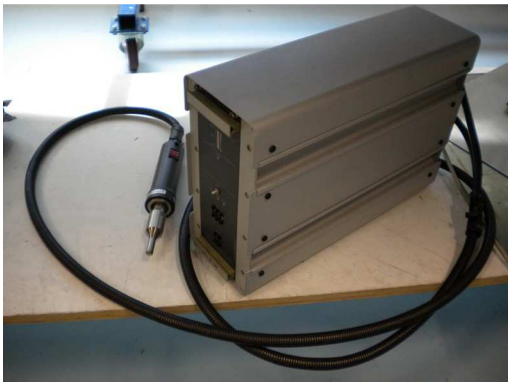

Fig.4.2 Rinco ultrasonic welder.

The next step of the process was hot-pressing in a Joos press machine (Fig.4.3). A standard cycle for PPS was set in the press (Fig.4.4). The values of pressure and temperature, desired and obtained during the processing of one of the panels are depicted in Fig.4.4.

Fig.4.3 Joos Press.

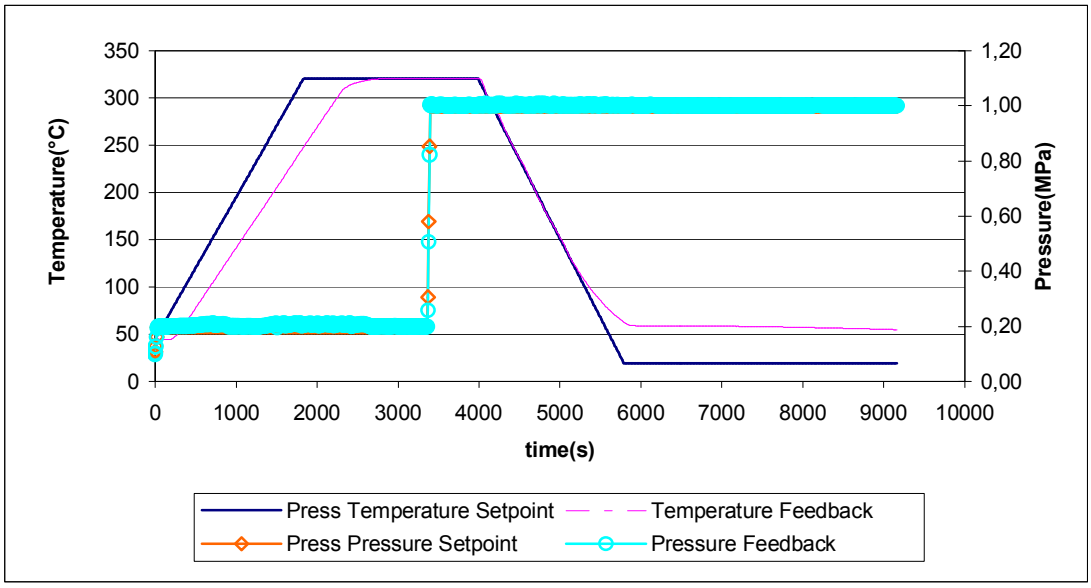

Fig.4.4 Standard cycle for PPS.

4.3 Quality control

With the purpose of checking the quality of the produced laminates, ultrasonic scanning (C-scan technique) was undertaken in a C-scan by Middas, with a transducer of 10 Mhz (Fig.4.5). An actual size map of the plate is generated after scanning associating a color to each ultrasonic attenuation level, which can be related with the surface finish and internal imperfections like voids, different cooling state of the matrix or waving of the fibers.

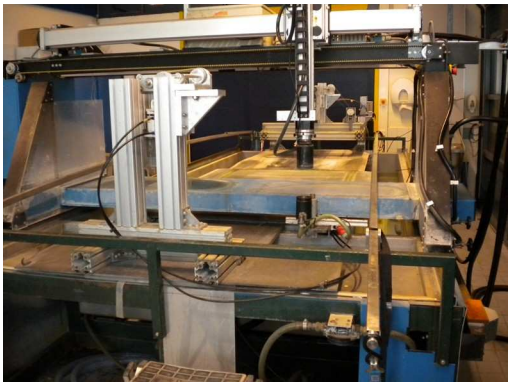

Fig.4.5 Middas C-scan.

The C-scan data were analysed with the Automated Laminate Inspection System (ALIS), designed for the ultrasonic evaluation of composites and fibre metal laminates. Areas of (28x54)cm^2 were checked and average value of attenuation and standard deviation were measured by the ALIS software. This area corresponds with the sections of the panels from where specimens in the warp direction, with a length between 25 and 28 cm, shall be cut (see Fig.4.6).

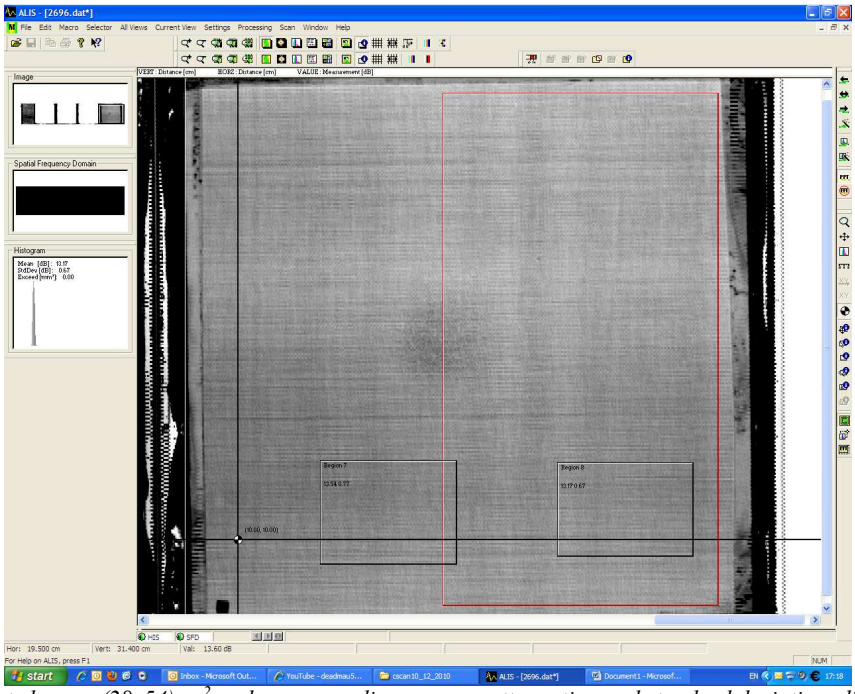

Fig.4.6 Tested areas (28x54)cm^2 and corresponding average attenuation and standard deviation displayed by ALIS on the left.

4.4 Cutting

The cutting was arranged depending on the results of the C-scan, the number of specimens to test, for each type of test and ageing condition, and the sizes according to the different standards used.

The data of the C-scan also were used to plan the cutting of the specimens. Those ones with the lowest attenuation were dedicated to bending testing and humidity uptake measurements. In these best panels, the area who presented less attenuation was given over to humidity uptake coupons and the rest to bending specimens. The next ones with less attenuation were fully used for in-plane shear testing. Finally the tensile test specimens were cut from the panels with the highest attenuation level. In this way, the effects of internal imperfections and surface finish were tried to be taken out of the analysis of humidity uptake. As far as more tensile results can be found in literature, the panel with the lowest quality was dedicated for tensile tests. Also having specimens for each kind of test cut from the same panel was considered.

A first cut of the panels, to get smaller pieces, was carried out in an open water-lubricated cutting machine depicted in Fig.4.7. The model was a BP 3515 by Carat. A delamination of 0.7 to 1 cm can be expected with the blade used. This delamination was taking in account, trying always to have a symmetric configuration of the specimen, keeping this delaminated zone in opposite transverse edges.

The cutting was finished in a water-lubricated precision sawing machine, a Unitom cutting machine produced by Struers (Fig.4.8).

Fig. 4.7 Carat open cutting machine.

Fig.4.8 Unitom cutting machine.

The blade was a high quality cut-off wheel, also by Struers, 10535, with a thickness of 2.5 mm. This thickness has to be taken into consideration, in order to calculate the number of specimens that can be obtained from a laminate. The speed of cutting was set at 0.75 mm/s.

4.5 Conditioning

For humidity uptake, the geometry and the sampling of the specimens recommended in ASTM D5229 (Ref.2.5) is explained in Appendix 1.

After cutting the specimens, the conditioning could be carried out. First of all, the specimens were dried for a week in a Vacuum Drying Chamber, model VTR, by Hezeus Instruments, at 60°C, maintaining the required uniform temperatures to within ±1°C (Fig.4.9).

The drying was undertaken according to procedure D from the standard ASTM D5229 (Ref.2.5). Procedure D covers the conditioning of material coupons to an essentially moisture-free condition, i.e. 'dry' state. This means that a general test coupon is held in an oven with a near-vacuum environment, with a prescribed elevated temperature until effective equilibrium is reached. The measurement of mass was taken daily.

Subsequently the ageing of the samples was carried out under procedure A of ASTM D5229 (Ref.2.5), to monitor moisture content, to calculate Fick's water diffusion coefficient and moisture content at equilibrium. The apparatus used was a WK111340 climate chamber of Weiss (Fig.4.10). The conditioning chamber was capable of maintaining the required uniform temperatures to within ±1°C and the vapor-level controlled, maintaining the required relative vapor level to within ±3%.

The conditions were 80°C and 90% RH in order to accelerate the humidity uptake, always below the glass transition temperature and with a temperature and humidity level as high as possible. The coupons were conditioned to dry state, one month of conditioning and two months of conditioning, , which is assumed to be the full saturated sample for testing.

Fig.4.9 Hezeus vacuum drying chamber.

Fig.4.10 Weiss climate chamber.

In order to work according to the standard the prescriptions below were followed.

A plastic sealable clean, dry chemical container with silica gel was used as desiccator, in which specimens being oven-dried shall be brought to laboratory temperature and stored following removal of the specimens from the oven

Sealable, flexible bag were used to transport the specimens from the climate chamber to the balance and there coupons were cooled down to room temperature prior to weighing.

The samples were not ever more than 30 minutes out of the climate chamber when they were weighed.

Any exuded or condensed moisture were cleaned from specimens with paper towels.

When handling specimens always clean, powder free gloves were worn.

The weighing was performed once a day within the 3 first days, since no recommendation is given by the ASTM D5229 for the weighing during the initial linear part of the humidity uptake curve. Later during the 2 month conditioning, weighing was performed once very week according to the recommendation of the ASTM D5229.

4.6 Humidity absorption curve fitting

The data of the weighing during conditioning was fitted, assuming fickian behaviour as explained in the previous 2.4 Humidity section. This is supported by the work by Chen-Chi et al for CF/PPS (Ref. 2.4). The same hypothesis was also assumed for GF/PPS.

The data from the weighing was treated using the curve fitting tool by Matlab with the implied non-linear least-square method and the models were the custom equations shown in Table 4.2 for CF/PPS and in Table 4.3 for GF/PPS. The first three points of the weighting, within 3 days of conditioning, were chosen for the linear fitting. The linear fitting model (see Table 4.2 and Table 4.3) is consistent with Eq.2.6 explained above, copied here for better understanding.

$$\frac{M - M_i}{M_\infty - M_i} = 4\left(\frac{D_z t}{h^2 \pi}\right)^{1/2}$$

Eq.2.6

Where M, the moisture content, corresponds with f(x) in the model. M_i, the initial moisture content is 0. M_∞ is the saturation moisture content, estimated by the experimental moisture content from the average value of the 5 humidity uptake specimens of each material after 2 months. This saturation moisture content was 0.169% for CF/PPS and 0.209% for GF/PPS. Variable x is the reduced time, (√t/h), where t is time and h is thickness. Finally parameter d is the unknown diffusion coefficient to measure, corresponding with D_z in Eq.2.6. The initial value of the model is:

$$f(0) = 0[\%]$$

The boundary condition of the parameter is:

$$0 < d < 0.02[mm^2 / h]$$

The upper limit of the diffusion coefficient is an overestimation out of previous data from the work by Chen-Chi et al. (Ref.2.4). In Chen-chi´s research a diffusion coefficient of 37.9×10^{-9} cm^2/s ($0.0136 mm^2/h$) was measured at 80ºC/75%RH of conditioning for CF/PPS. This overestimation seemed to be consistent with the results found, which will be exposed in the corresponding 5.3 Humidity uptake fitting section below.

Matlab provides values with 95% confidence bounds for the measured parameter d.

The rest of the weighing data till the end of the conditioning were fitted with the curve fitting model (see Table 4.2 and Table 4.3). This model is consistent with Eq.2.5 explained above and copied here for better understanding.

$$\frac{M - M_i}{M_\infty - M_i} = 1 - \frac{8}{\pi^2}\exp\left(-\frac{\pi^2 D_z t}{h^2}\right)$$

Eq.2.5

Where M, the moisture content, corresponds with f(x) in the model. M_i, the initial moisture content is 0. M_∞ is the saturation moisture content, corresponding with parameter yi in the model. Variable x is the reduced time, (√t/h), where t is time and h is thickness. Finally parameter d corresponds with D_z in Eq.2.5. In this part of the fitting it was decided to leave yi and d as parameters to observe the behaviour of the fitting assuming Fick's law. The boundary conditions of this model are:

$$0 < yi < 0.3[\%]$$
$$0 < d < 0.02[mm^2 / h]$$

In this case the upper limit for yi comes from an overestimation of the measured saturation moisture content, 0.169% for CF/PPS and 0.209% for GF/PPS. The upper limit for d is already explained previously for the linear fitting model. Matlab provides values with 95% confidence bounds for the measured parameters yi and d.

The explained linear and curve fitting models are schemed in Table 4.2 in the case of CF/PPS and Table 4.3 in the case of GF/PPS.

Table 4.2 Linear and curve fitting of CF/PPS humidity uptake data.

Linear fitting	**Curve fitting**
FIck's solution for initial time	**Fick´s solution for ulterior time**
$\frac{M-M_i}{M_\infty-M_i}=4\left(\frac{D_z t}{h^2\pi}\right)^{1/2}$	$\frac{M-M_i}{M_\infty-M_i}=1-\frac{8}{\pi^2}\exp\left(-\frac{\pi^2 D_z t}{h^2}\right)$
General model:	**General model:**
f(x) = d^0.5*4*0.169*pi^(-0.5)*x f(x)=moisture content[%] d=linear fitting estimation of diffusion coefficient[mm^2/h] 0.169=experimental estimation of saturation moisture content from the average of the moisture content of the 5 tested specimens after 2 months[%] x=reduced time [h^0.5/mm]	f(x) = yi*(1-8/pi^2*exp(-pi^2*d*x^2)) yi=estimation of saturation moisture content out of the curve fitting[%] d= estimation of diffusion coefficient out of the curve fitting[mm^2/h]

Table 4.3 Linear and curve fitting of GF/PPS humidity uptake data.

Linear fitting	**Curve fitting**
FIck's solution for initial time	**Fick´s solution for ulterior time**
$\frac{M-M_i}{M_\infty-M_i}=4\left(\frac{D_z t}{h^2\pi}\right)^{1/2}$	$\frac{M-M_i}{M_\infty-M_i}=1-\frac{8}{\pi^2}\exp\left(-\frac{\pi^2 D_z t}{h^2}\right)$
General model:	**General model:**
f(x) = d^0.5*4*0.209*pi^(-0.5)*x f(x)=moisture content[%] d=linear fitting estimation of diffusion coefficient[mm^2/h] 0.209=experimental estimation of saturation moisture content from the average of the moisture content of the 5 tested specimens after 2 months[%] x=reduced time [h^0.5/mm]	f(x) = yi*(1-8/pi^2*exp(-pi^2*d*x^2)) yi=estimation of saturation moisture content out of the curve fitting[%] d= estimation of diffusion coefficient out of the curve fitting[mm^2/h]

4.7 Mechanical testing

After the selected ageing condition was reached, the specimens were taken out of the or vacuum oven or climate chamber to perform the three types of mechanical tests: tensile, in-plane shear and three point bending.

4.7.1 Tensile tests

Tensile tests followed recommendations of the ASTM D3039 (Ref.4.2). The geometry and the sampling of specimens for tensile testing are explained in Appendix 2. The estimation of tensile properties to measure and consequently the choice of apparatus are explained in Appendix 3.
The values that can be obtained from this test are: the ultimate tensile strength (UTS), the ultimate strain and the chord modulus of elasticity.
The sample, having a constant rectangular cross section, is mounted in the mechanical grips of the Zwick 250KN testing machine and loaded in tension, while recording force versus strain. An extensometer was utilized as strain-indicating device. An environmental chamber when needed was set at 80°C and 120°C within ±3°C (Fig.4.11). A thermo-couple set was also connected, attached to the specimen to assure that the reached temperature in the specimen was the same as the desired one.

Fig. 4.13 Zwick 250KN testing machine, mechanical grips, extensometer and environmental chamber,

In the beginning paper tabs, (80x200 mm), glued with Loctite 4062 cyano-acrilate instantaneous adhesive of Henkel were used. Slipping in the grips and detaching of the tabs, in the case of CF/PPS system, lead to carry out the subsequent tests without tabs. No differences in data scatter appeared due to testing without tabs.

The thickness and width of the test specimen were measured with a caliper, with an accuracy of 0.05 mm, on three different points within ±1 cm of the centre of the specimen and the averages were calculated. This procedure was followed in the rest of mechanical tests.

The test speed was 2mm/min, the standard speed for constant head-speed tests prescribed by the standard.

The tensile stress and UTS are calculated according to Eq.4.1 and Eq.4.2 (Ref. 4.2):

$$\sigma_i = P_i / A$$

σ_i= tensile stress at ith data point, MPa

P_i= load at ith data point, N

A= average cross-sectional area, mm^2

Eq.4.1

$$UTS = P^{max} / A$$

UTS= ultimate tensile strength, MPa

P^{max}= maximum load before failure, N

Eq.4.2

The tensile chord modulus of elasticity (E-modulus) must be determined between 1000 με and 3000 με of strain by Eq.4.3 (Ref.4.2):

$$E^{chord} = \Delta\sigma / \Delta\varepsilon$$

E^{chord}= tensile chord modulus of elasticity, GPa

$\Delta\sigma$= difference in applied tensile stress between 1000 με and 3000 με strain points, MPa

$\Delta\varepsilon$= difference between the two strain points (nominally 0.002)

Eq.4.3

For each series of tests the average and the coefficient of variation in percent of each property were calculated according to the standard (Ref.4.2).
Also the minimum and the maximum data were depicted in graphs. These statistics were calculated for the other mechanical tests.

4.7.2 In-plane shear tests

The in-plane shear tests were based on the ASTM D3518 (Ref.4.1). The geometry and the sampling of specimens for in-plane shear testing are explained in Appendix 4. The estimation of in-plane shear properties to measure and consequently the choice of apparatus are explained in Appendix 5.
This test method is useful for determining the in-plane shear strain response, including the in-plane shear modulus and strength. Using strain measuring devices to record the induced strain of the test material, the values that can be obtained are:

- The shear stress versus shear strain response;
- In- plane shear modulus of elasticity;
- Maximum in-plane shear stress for a ±45˚ laminate;
- Maximum in-plane shear strain for a ±45˚ laminate.

The coupon is mounted in the mechanical grips of the Zwick 250KN (Fig.4.14) and loaded in tension, while recording load, longitudinal strain and lateral strain by means of strain gages. Also, an extensometer was used in the longitudinal direction. The supplier was Kyowa strain gages. The model was a KFG-5-120-C1-23, a general-purpose foil strain gage, with a length of 5 mm and a gage factor of 2.12 at (24°C/50%RH).

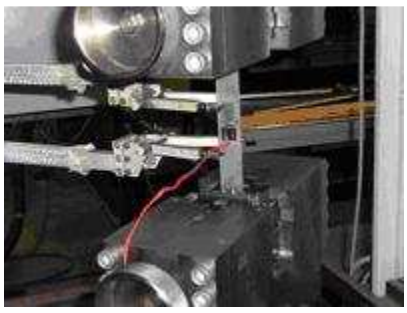

Fig.4.14 Mechanical Grips often used in the 250 KN Zwick..

The speed of testing was 0.02 mm/min, according to ASTM D3039 as no recommendation is given in the specific standard for in-plane shear.
The in-plane shear stress, its maximum, the shear strain and its maximum were calculated according to the following formulas (Ref.4.1):

$\tau_{12}^{i} = P_i / 2A$

τ_{12}^{i} = shear stress at i-th data point, MPa

P_i = load at i-th data point, N

A = cross-sectional area in accordance with Test Method D 3039/D 3039M, mm^2

Eq.4.4

$\tau_{12}^{m} = P^m / 2A$

τ_{12}^{m} = maximum in-plane shear stress, MPa

P^m = maximum load at or below 5 % shear strain, N

Eq.4.5

$$\gamma_{12i} = \epsilon_{x_i} - \epsilon_{y_i}$$

$$\gamma_{12}^{m} = \min\{\gamma_{12}\}_{\text{at maximum shear stress}}^{5\,\%}$$

where:

γ_{12_i} = shear strain at *i*-th data point, με;

ϵ_{x_i} = longitudinal normal strain at *i*-th data point, με; and

ϵ_{y_i} = lateral normal strain at *i*-th data point, με; and

γ_{12}^{m} = maximum shear strain, με.

Eq.4.6

The shear chord modulus of elasticity (G-modulus) must be determined out of the curve shear stress versus shear strain, corresponding to a shear strain range of 4000 ±200 με, starting with the lower strain point in the range of 1500 to 2500 με of shear strain by Eq.4.7 (Ref.4.1):

$G_{12}^{chord} = \Delta\tau_{12} / \Delta\gamma_{12}$

G_{12}^{chord} = shear chord modulus of elasticity, GPa

$\Delta\tau_{12}$ = difference in applied shear stress between 2000 με and 6000 με shear strain points, MPa

$\Delta\gamma_{12}$ = difference between the two shear strain points (nominally 0.004)

Eq.4.7

4.7.3 Three point bending tests

The three point bending tests were carried out according to the ASTM D7264 standard (Ref.4.3). This standard describes the procedure to test the flexural stiffness and strength properties of polymer matrix composites.

The three point bending flexural tests provide values for the flexural modulus, flexural strength and the flexural stress-strain response of the material under investigation

The main advantage of the three point bending test method is the ease of test specimen preparation and testing. Disadvantages include: stress concentrations and secondary stresses may occur at the loading points, and the results are sensitive to specimen and loading geometry and strain rate. This test method is often used for quick assessment of the quality and performance of the composite material.

Before initiating the test, the geometry of the specimens and the sampling (see Appendix 6) and the expected value of the maximum load from the data supplied by Tencate (see Appendix 7) were calculated.

The Zwick 20KN testing machine was used, with the three point bending setup and the appropriate loading nose and supports with a radius of 3.0 mm ±0.1 mm (Fig.4.15, Ref.4.3).

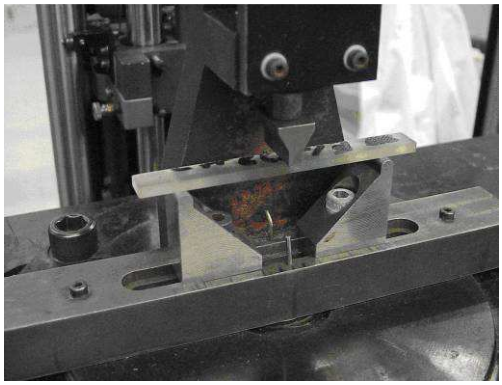

Fig.4.15Three point bending fixture.

The test specimens were centered on the supports and it was ascertained that the support span and the test specimen were parallel. The test speed of the loading nose was 1mm/min.

The following calculations were done for the flexural stress at the outer surface at mid-span (Eq.4.8), flexural strength (Eq.4.9) and flexural chord modulus (Eq.4.10) in accordance with the standard (Ref.4.3).

$$\sigma = \frac{3PL}{2bh^2}$$

σ= stress at the outer surface at mid-span, MPa

P= applied force, N

L= support span, mm

b= width of beam, mm

h= thickness of beam, mm

Eq.4.8

$$\sigma^m = \frac{3P^mL}{2bh^2}$$

σ^m = maximum stress at the outer surface at mid-span, MPa

P^m = maximum applied force, N

Eq.4.9

$$E_f^{chord} = \frac{\Delta\sigma}{\Delta\varepsilon}$$

E_f^{chord} = flexural chord modulus of elasticity, MPa

$\Delta\sigma$ = difference in flexural stress between 0.001 and 0.003 strain points, MPa

$\Delta\varepsilon$ = difference between the two selected strain points (nominally 0.002)

Eq.4.10

The maximum strain at the outer surface also occurs at the mid-span and is calculated as follows (Ref.4.3):

$$\varepsilon = \frac{6\delta h}{L^2}$$

ε = maximum strain at the outer surface, mm/mm

δ = mid-span deflection, mm

Eq.4.11

4.8 Microscopic analysis

Once the material was conditioned for two months, the non-tested dry and 2-months-conditioned materials of both systems were inspected in a field emission scanning electron microscope (SEM), JEOL JSM-7500F. The energy dispersive system that provides energy dispersive X-ray spectroscopy (EDS), allowed the search of oxygen groups which indicate presence of the absorbed water. Windows of 42.4μmx60μm at 2000x magnification (Fig.4.16) were tested inside the material (Fig.4.17) to check pure dry material, and later to check if the material is saturated in the middle of the cross section after 2-month conditioning. Also the edge was tested to compare the content of oxygen groups at the surface to that found inside.

Also micrographs were taken of the tensile tested dry and 2-month conditioned material at room temperature, and at 120°C. The in-plane shear tested specimens were analysed as a matrix dominant test. In this case specimens of in-plane shear tested dry and 2-month conditioned material were examined.

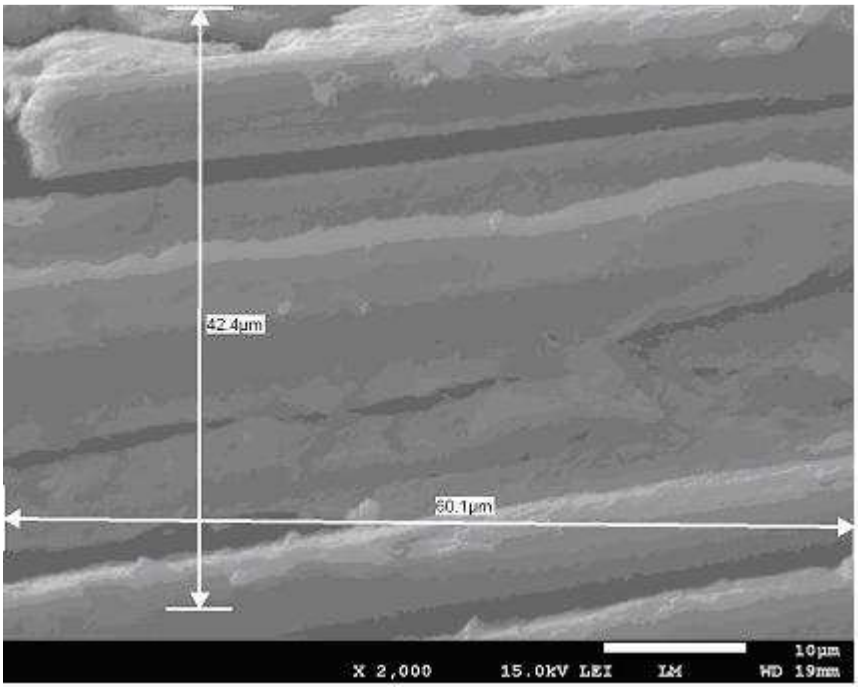

Fig.4.16 Definition of the area for EDS.

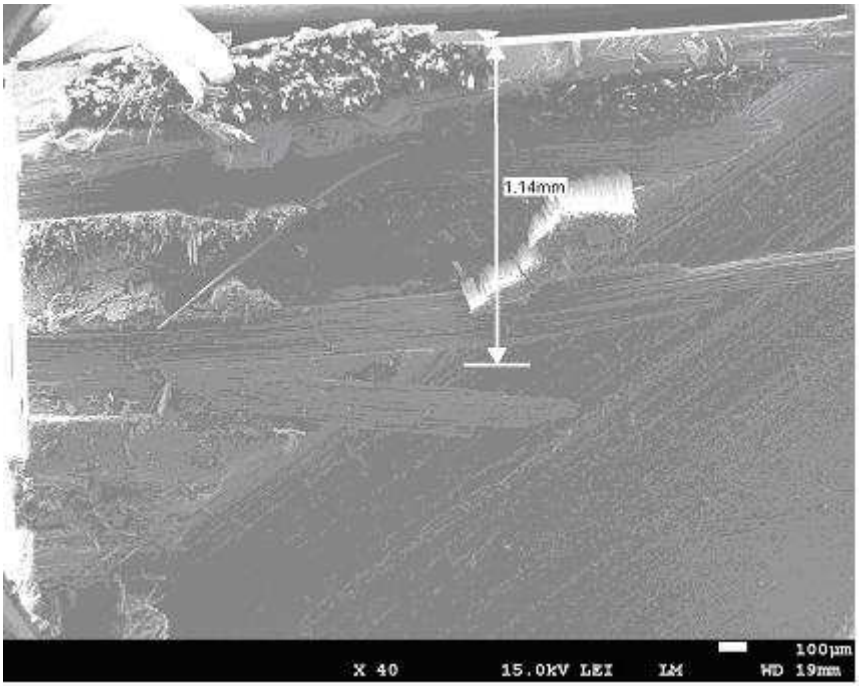

Fig.4.17 Location of the SEM analysis 1.14 mm inside of a carbon specimen with 2.38 mm thickness.

CHAPTER 5: RESULTS

In this chapter the results from the different steps of the research can be found and are interpreted.

5.1 Hot-pressing monitoring

The hot-pressing data revealed that the requested temperature profile was followed apart from the thermal inertia in the heating ramp and in the cooling. In the pressure profile, failures in the pressing were found but no influence on the quality was observed in the C-scan results. In the first processed panel, a short processing of 7000 seconds was used and as also pressure failures were found, worse attenuation values were observed (see Fig.5.1).

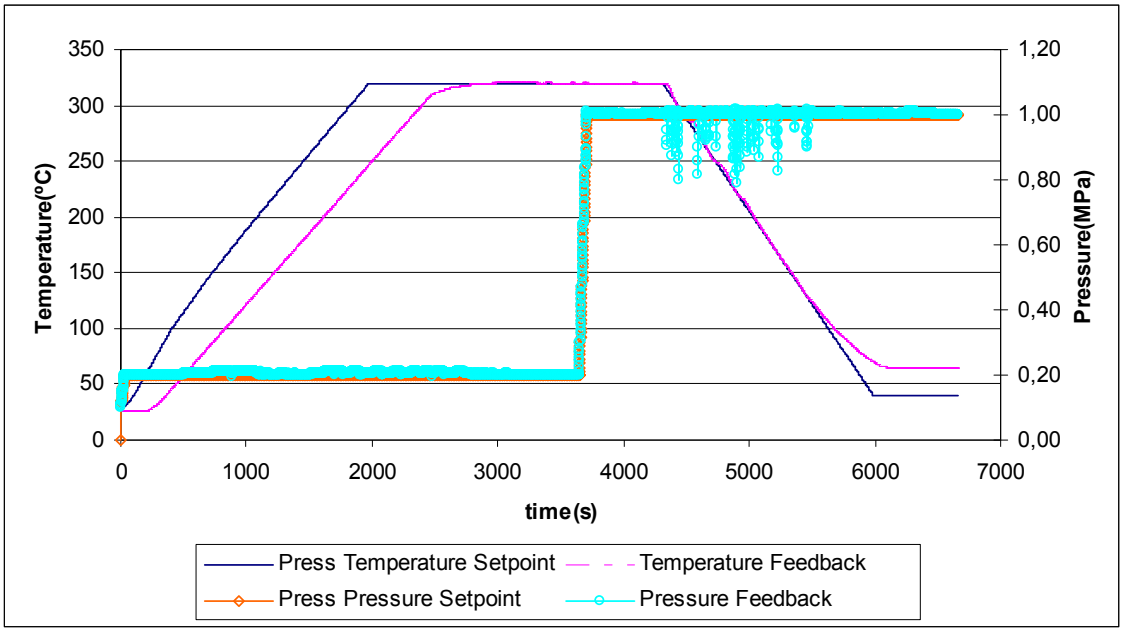

Fig.5.1 Thermal inertia in heating and cooling ramp and pressing failures of the first processed panel.

When pressure failures happened, longer times of cooling down under pressure seemed to compensate the pressing failure (Fig.5.2). Homogeneous laminates were obtained and no leaking of resin during the hot pressing was observed.

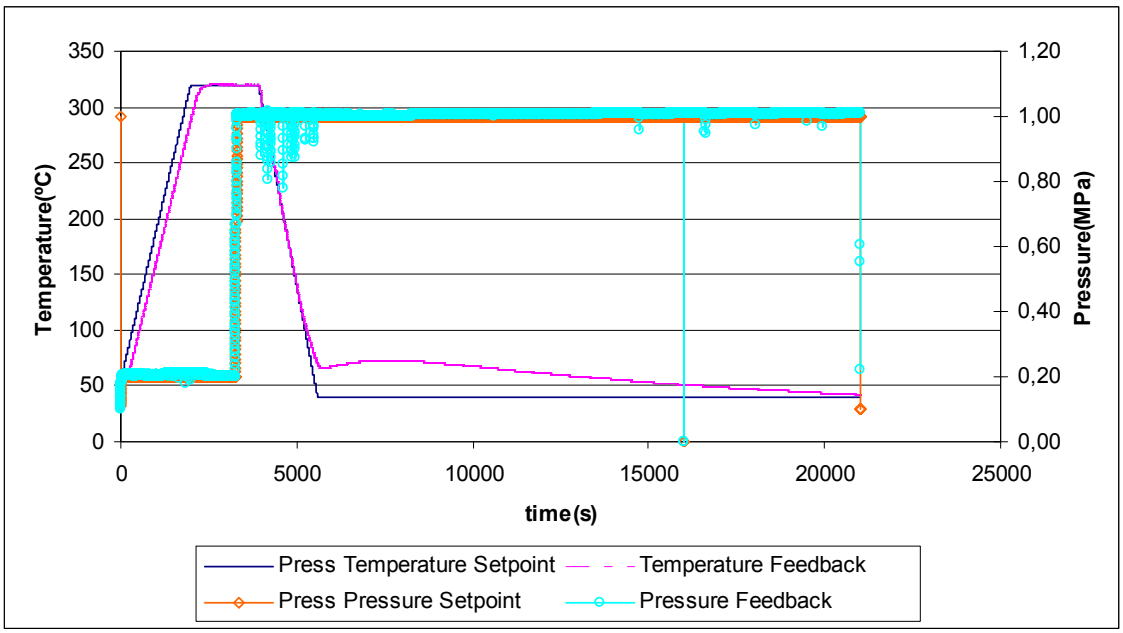

Fig.5.2 Cycle of 20000 s.

5.2 C-Scan analysis

The C-Scan data were analysed with the Automated Laminate Inspection System (ALIS), designed for the ultrasonic evaluation of composites and fibre metal laminates, as explained in 4.3 Quality control section. As an example of the performed analysis in Fig.5.3 a first batch of five laminates is displayed. The first piece on the left is a template of material used to calibrate the apparatus, the next three ones on the left are CF/PPS and the fourth one is GF/PPS. The average attenuation of the carbon system was low enough (average=4.8dB and average standard deviation=1.09dB of the analysed areas (28x54) cm^2. Usually for 8 layers of CF/PPS attenuations of 4±2dB are measured (Ref.5.1). Standard deviations of 1dB or less are acceptable (Ref.5.1). In the case of GF/PPS, the average attenuation was also low enough (average=12.08dB and average standard deviation=0.61dB of the analysed areas (28x54) cm^2. Usually for 8 layers of GF/PPS attenuations of 10±2dB are measured (Ref.5.1).

The homogenous of the attenuation levels showed that the whole panel could be used for cutting specimens. Two centimetre width lateral strips along the edges were rejected in order to avoid side effects.

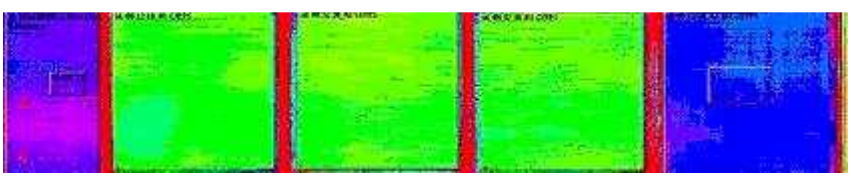

Fig.5.3 First batch of 4 laminate results. From left to right, template, 3 CF/PPS and 1 GF/PPS.

5.3 Humidity uptake fitting

The two Fick's properties of the humidity absorption, the diffusion coefficient and the saturation level, were derived in this section as explained in the previous 4.6 Humidity absorption curve fitting section. Also the goodness of the fits is provided out of the Matlab analysis.

Fig.5.4 and Fig.5.5 display the experimental moisture absorption data, the linear and curve fitting models, and their corresponding upper and lower evaluations with ±95% confidence levels (CL) of the parameters of the models for CF/PPS and GF/PPS, for one specimen in each case.

Table 5.1 and Table 5.2 show the linear and curve fitting models explained earlier, for one of the specimens of each material, corresponding to the plotted data in Fig.5.4 and Fig.5.5 The parameters obtained from both fittings, the 95% CL intervals for the fitted parameters, and the goodness of the fits are also included in the same tables.

Averages and variation coefficients values of the estimation of the diffusion coefficient out of the linear fitting for five specimens of each material, as it is recommended to be calculated in the ASTM standard D5229 (Ref.2.5), are shown in Table 5.3.

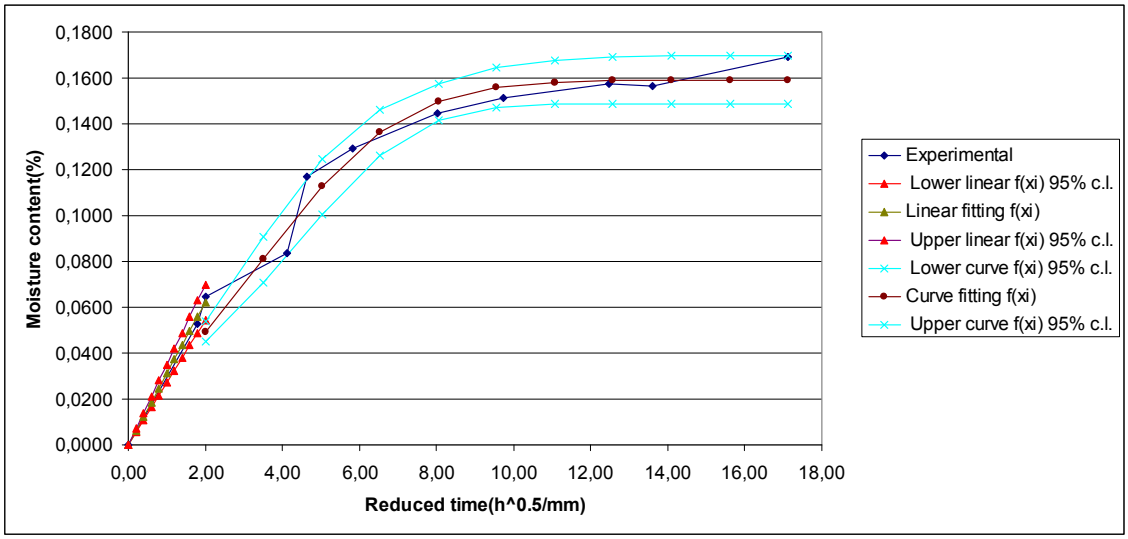

Fig. 5.4 Experimental moisture absorption data, linear and curve fittings and upper and lower evaluations of the fittings with ±95% C.L. of the parameters in the case of CF/PPS.

Table 5.1 Fittings and goodness of the fits of CF/PPS moisture absorption.

Linear fitting	**Curve fitting**
General model:	General model:
f(x) = d^0.5*4*0.169*pi^(-0.5)*x f(x)=moisture content[%] d=linear fitting estimation of diffusion coefficient[mm^2/h] 0.169=experimental estimation of saturation moisture content from the average of the moisture content of the 5 tested specimens after 2 months[%] x=reduced time [h^0.5/mm]	f(x) = yi*(1-8/pi^2*exp(-pi^2*d*x^2)) yi=estimation of saturation moisture content out of the curve fitting[%] d= estimation of diffusion coefficient out of the curve fitting[mm^2/h]
Coefficients (with 95% confidence bounds):	**Coefficients (with 95% confidence bounds):**
d = 0.006627 (0.004955, 0.008299)	d = 0.004096 (0.002801, 0.005391)
	yi = 0.1591 (0.1486, 0.1696)
Goodness of fit:	**Goodness of fit:**
SSE: 1.194e-005	SSE: 0.0004284
R-square: 0.9949	R-square: 0.921
Adjusted R-square: 0.9949	Adjusted R-square: 0.9079
RMSE: 0.002444	RMSE: 0.00845

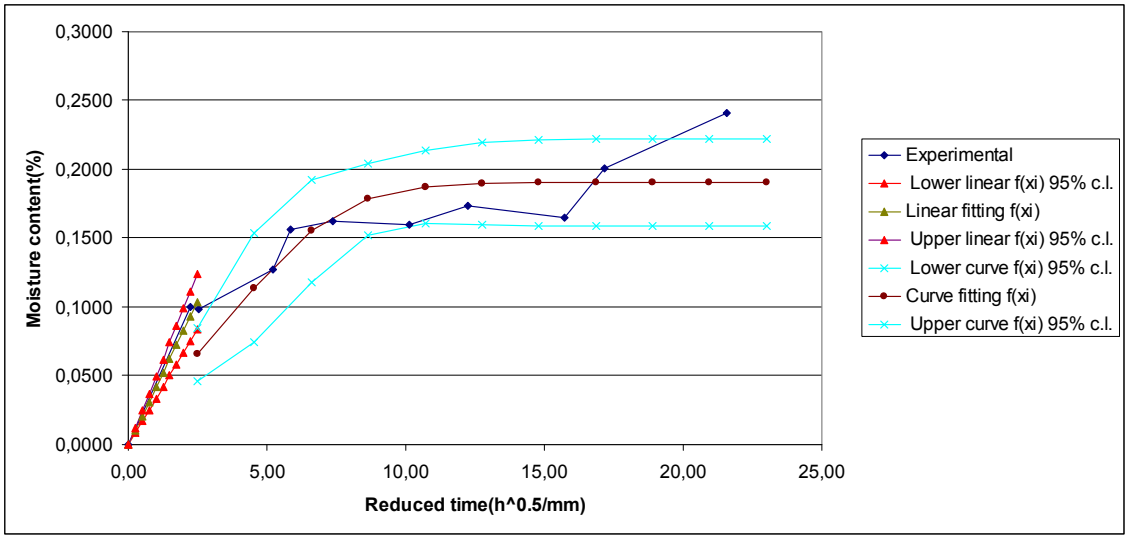

Fig. 5.5 Experimental moisture absorption data, linear and curve fittings and upper and lower evaluations of the fittings with ±95% C.L. of the parameters in the case of GF/PPS.

Table 5.2 Fittings and goodness of the fits of GF/PPS moisture absorption.

Linear fitting	**Curve fitting**
General model:	General model:
f(x) = d^0.5*4*0.209*pi^(-0.5)*x f(x)=moisture content[%] d=linear fitting estimation of diffusion coefficient[mm^2/h] 0.209=experimental estimation of saturation moisture content from the average of the moisture content of the 5 tested specimens after 2 months[%] x=reduced time [h^0.5/mm]	f(x) = yi*(1-8/pi^2*exp(-pi^2*d*x^2)) yi=estimation of saturation moisture content out of the curve fitting[%] d= estimation of diffusion coefficient out of the curve fitting[mm^2/h]
Coefficients (with 95% confidence bounds):	**Coefficients (with 95% confidence bounds):**
d = 0.007729 (0.00472, 0.01074)	d = 0.003451 (0.0004028, 0.006498)
	yi = 0.1903 (0.1586, 0.222)
Goodness of fit:	**Goodness of fit:**
SSE: 8.065e-005	SSE: 0.004465
R-square: 0.9878	R-square: 0.4517
Adjusted R-square: 0.9878	Adjusted R-square: 0.3603
RMSE: 0.00635	RMSE: 0.02728

Table 5.3 Average diffusion coefficient and its variation coefficient of the 5 specimens out of the linear fitting. Also Average R-square and its variation coefficient of the goodness of the linear fitting.

	Diffusion coefficient(mm^2/h)	Coefficient of variation (%)	Average R-square	Coefficient of variation (%)
CF/PPS	0,0054	35,13	0,93	11,01
GF/PPS	0,0097	37,15	0,95	4,31

In composite industry, a value of 5% of coefficient of variation denotes a good repeatability of the measurement. It is clear that the use of only three points in the linear fitting is not sufficient to avoid experimental scattering. The fact that the humidity uptake of this composite is so low and the data was scattered showed that on one hand more mass should be used as prescribed in the standard. And on the other hand, the error of the weighting procedure, bigger than the balance accuracy, shall be used to round off the weighing data. The weighing procedure error is calculated in Appendix 8. The weighing method error was ±10 mg, much more than the accuracy of the balance used to round off every measurement (±0.1mg).

Comparing the estimated parameters in the linear fitting to those obtained in the curve fitting, it can be concluded that the curve fitting underestimated the diffusion coefficient although an accurate estimation of the humidity saturation was achieved. These results support the Fickian diffusion behaviour of the studied composites.

The diffusion coefficient of the GF/PPS system was higher than the one of CF/PPS, while the order of magnitude is similar. Furthermore, the thickness of the 8 layers of each material is different. Although the diffusion coefficient is only dependent on temperature in Fick's theory, more research is needed to control and compare the influence of the thickness on diffusion coefficient measurement. Other variables that could influence on this coefficient and were not controlled in this research are degree of crystallinity, fiber fraction or the sizing used in fibers.

The same can be said about the saturation level. A higher level of saturation humidity uptake was found in GF/PPS.

The low level of humidity uptake of PPS composite is remarkable. A 0.169% and 0.209% saturation level at 80ºC and 90%RH were measured for carbon and glass composites respectively. This is comparable to the humidity uptake of PEEK, 0.153% at 80"C, 85 %RH by Chen-chi (Ref.2.4). In the work by Chen-chi CF/PPS reached a saturation level of 0.138% at 80ºC, 85%RH.

5.4 Mechanical testing data

5.4.1 Tensile test results

The change in tensile stiffness and strength with the time of conditioning and the temperature of testing is depicted in Fig.5.6, Fig.5.7 for CF/PPS and Fig.5.8 and Fig.5.9 for GF/PPS, compared to the values measured by the supplier, Tencate, when data were available (Ref.3.1). Minimum, maximum and average values of the magnitudes when tests ran in an acceptable way are shown. When only one specimen could be taken as a good measurement, no error bar could be shown.

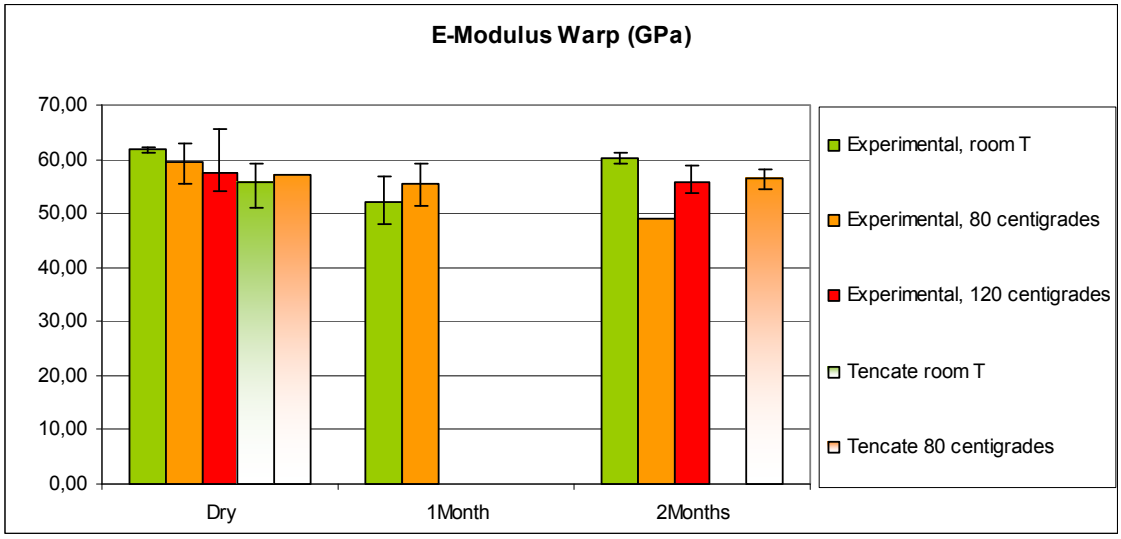

Fig.5.6 Change in E-modulus with time of conditioning and testing temperature for CF/PPS.

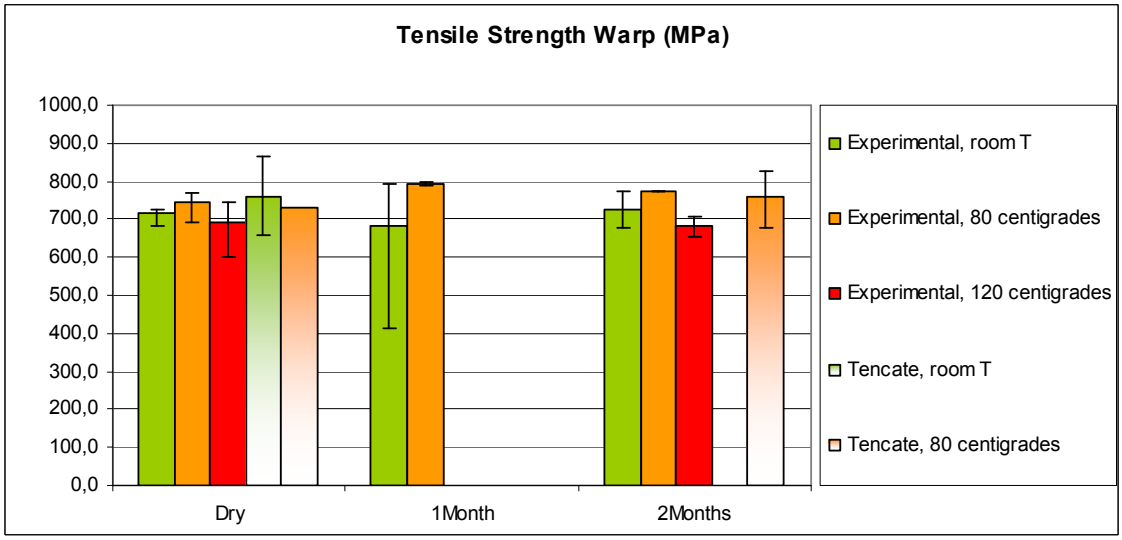

Fig.5.7 Change in tensile strength with time of conditioning and testing temperature for CF/PPS

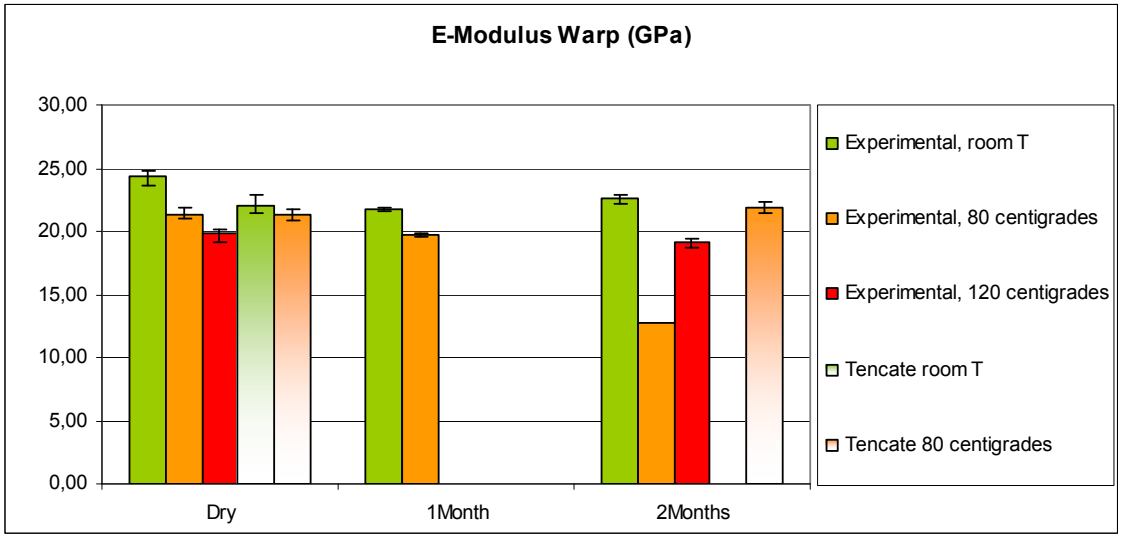

Fig.5.8 Change in E-modulus with time of conditioning and testing temperature for GF/PPS.

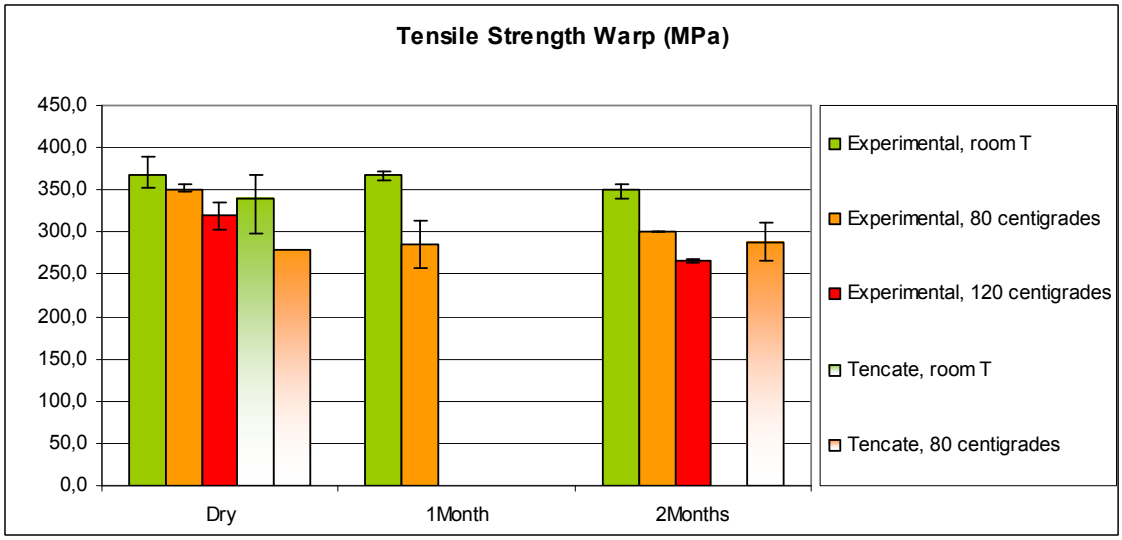

Fig.5.9 Change in tensile strength with time of conditioning and testing temperature for GF/PPS.

Tensile tests show a fiber dominant behaviour. Since the fibers themselves are not damaged by the humidity uptake, a remarkable retention of properties was observed after two months of conditioning in a harsh environment. Losses of properties of less than 10% were found. Higher levels of loss of properties for GF/PPS were obtained when compared to CF/PPS. This fact can signify that the interface or the fiber in the case of GF/PPS is more sensitive to humidity, which is consistent with Jirui Chen´s results, explained above in. 2.5.2 Effect of environment on the PPS composite mechanical properties section.

At elevated temperatures, softening of the matrix caused that the tensile properties decreased when material was tested above Tg of PPS (90ºC) as explained in 2.3 Temperature section. It is

interesting to observe the different scale of time of humidity and temperature effects. Meanwhile the humidity uptake effect was observed after 2 months of conditioning, the effect of temperature was observed in the testing time. The fact that the CF composite is more resistant to temperature in a dry condition might indicate a weaker interface of the GF composite since both systems have the same matrix, which is exposed to the same temperature above Tg.

The tested tensile specimens, for all conditions of ageing and temperature are shown in Fig. 5.10. Please note the inappropriate failure of the CF/PPS in the gripping zone and the change in the use of paper tabs. As the data obtained matched with the data by Tencate, and acceptable data of variation was achieved, in spite of the fact that failure zone was not located in the gauge zone in many cases, especially for CF/PPS, the experimental data obtained can be accepted.

Fig. 5.10 Tensile tested specimens.

5.4.2 Three point bending results

The change in flexural modulus and strength with the time of conditioning is depicted in Fig.5.11, Fig.5.12 for CF/PPS and Fig.5.13 and Fig.5.14 for GF/PPS, compared to the values measured by the supplier, Tencate, when data were available (Ref.3.1). Minimum, maximum and average values of the magnitudes are shown.

Checking the results of flexural testing, a matrix and matrix interface dominant behaviour, the strength of the CF/PPS interface even after being hydrothermally affected, becomes clear. On the other hand the loss of flexural strength of the GF/PPS is 25%. This data is consistent with that one exposed by Jirui-Chen. At 95°C, a 40% glass reinforced PPS shows a reduction of more than 30% in flexural strength after a five-week exposure period. The same PPS material but unreinforced shows no change in flexural strength with exposure to water (Ref. 2.7 p.10). It can be concluded that the interface between the GF and PPS is sensitive to water absorption. In flexural testing, this influence could be observed clearly. It can be anticipated that a more sensitive interface to water attack can be found in GF/PPS.

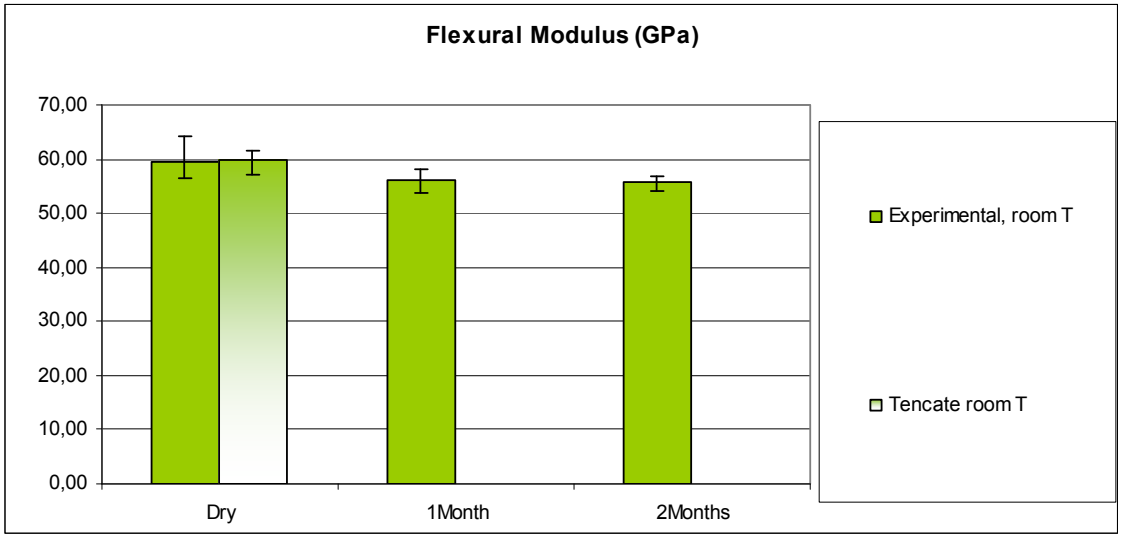

Fig.5.11 Change in flexural modulus of elasticity with time of conditioning for CF/PPS.

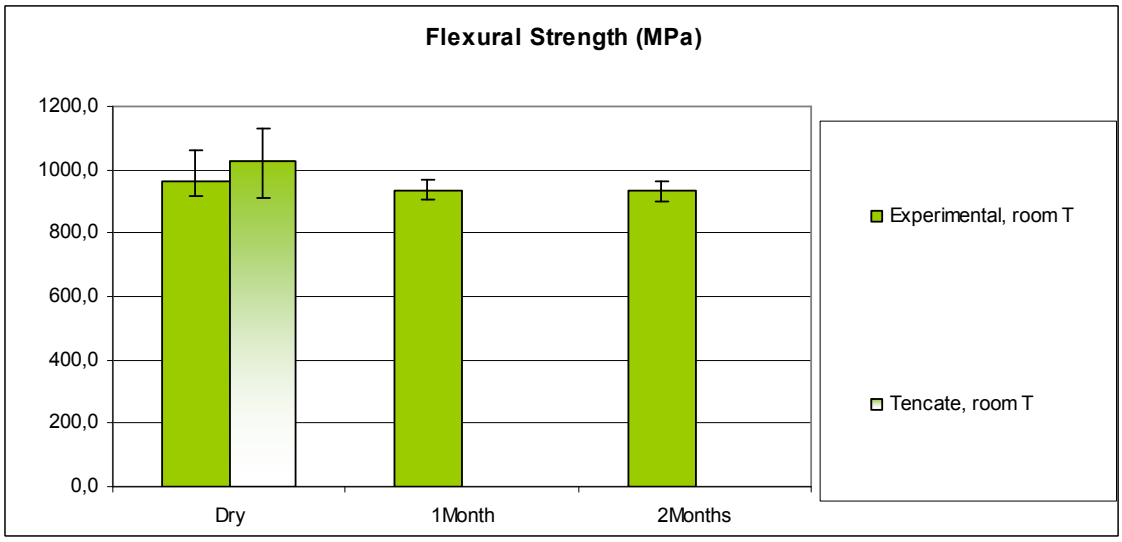

Fig.5.12 Change in flexural strength with time of conditioning for CF/PPS.

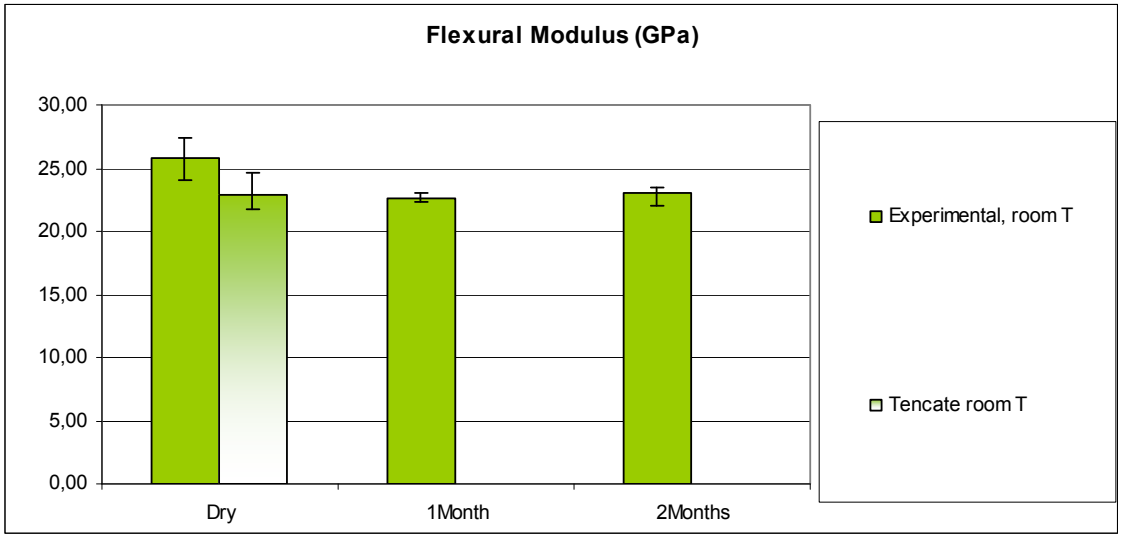

Fig.5.13 Change in flexural modulus of elasticity with time of conditioning for GF/PPS

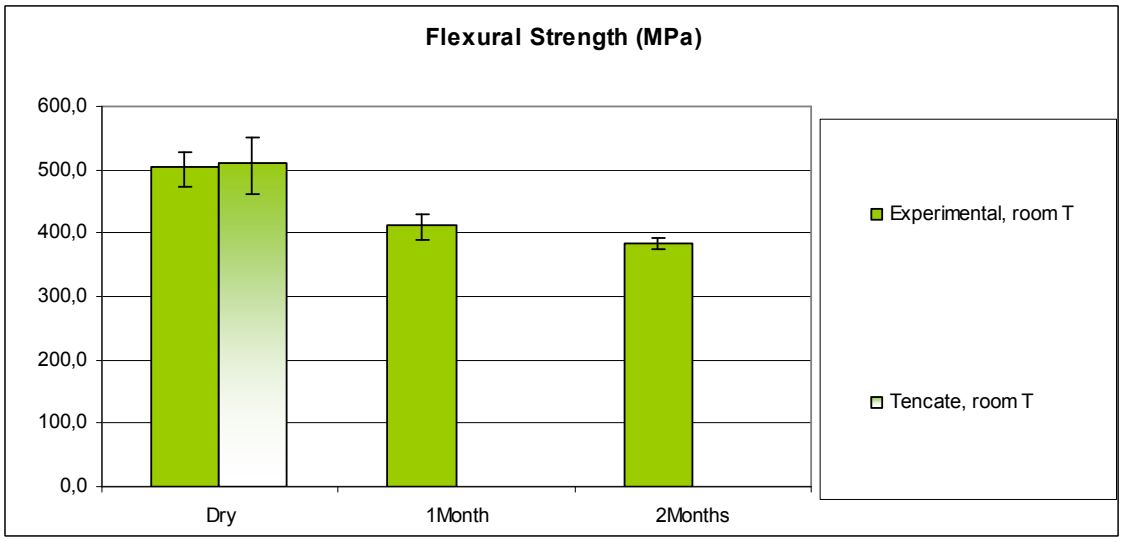

Fig.5.14 Change in flexural strength with time of conditioning for GF/PPS

The tested three-point bending specimens, for all conditions of ageing are shown in Fig.5.15. The test specimen failure always occurred on the outer surface in the tension side.

Fig. 5.15 Three-point bending tested specimens.

5.4.3 In-plane shear results

The change in in-plane shear modulus and strength with the time of conditioning is depicted in Fig.5.16, Fig.5.17 for CF/PPS and Fig.5.18 and Fig.5.19 for GF/PPS, compared to the values measured by the supplier, Tencate, when data were available (Ref.3.1). Minimum, maximum and average values of the magnitudes are shown. Tencate takes the in-plane shear strength as the corresponding stress for the maximum force measured, while the used standard for experimental data obtained recommends taking a value at a 5% of shear strain if this value is exceeded. As both values of strengths can be calculated with the recorded data, both calculated strengths are depicted as experimental, according to ASTM D 3518, and experimental (Tencate criteria).

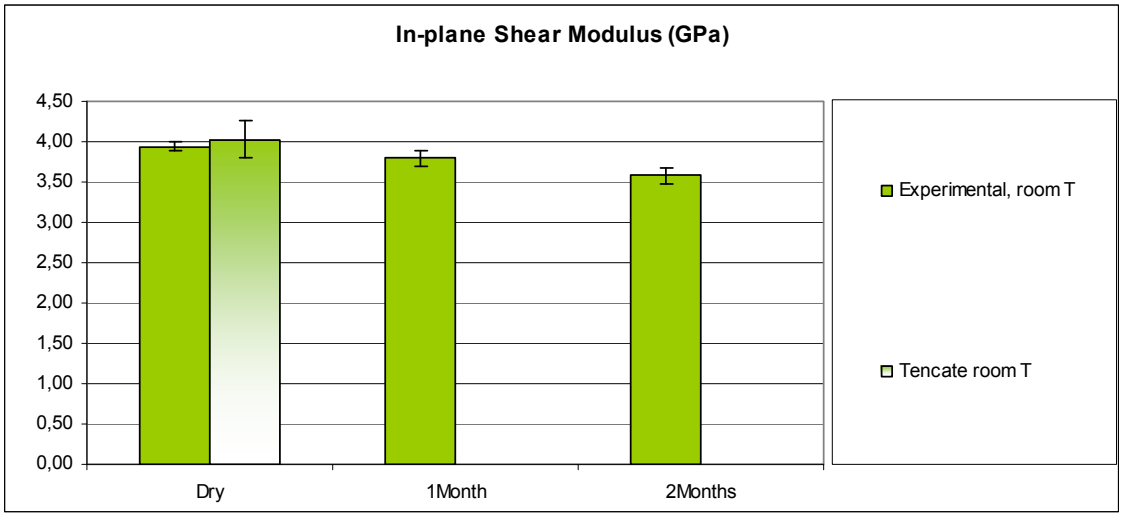

Fig.5.16 Change in in-plane shear modulus with time of conditioning for CF/PPS.

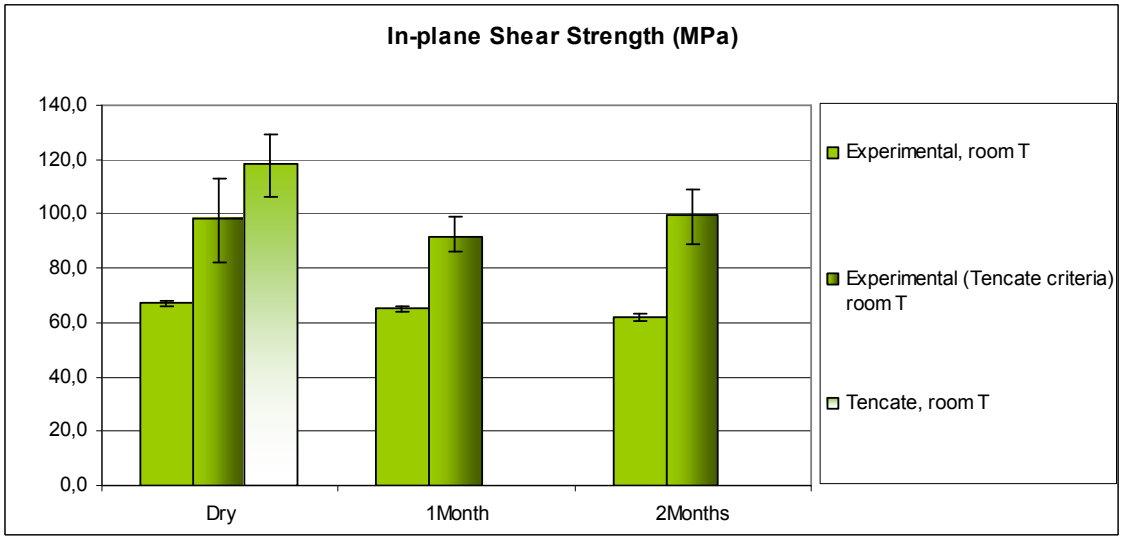

Fig.5.17 Change in in-plane shear strength with time of conditioning for CF/PPS.

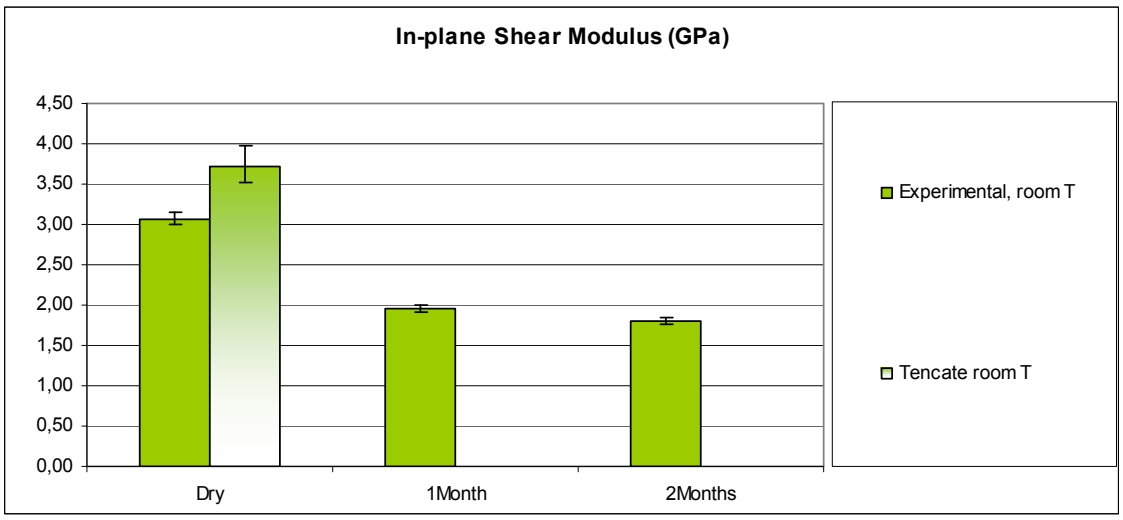

Fig.5.18 Change in in-plane shear modulus with time of conditioning for GF/PPS.

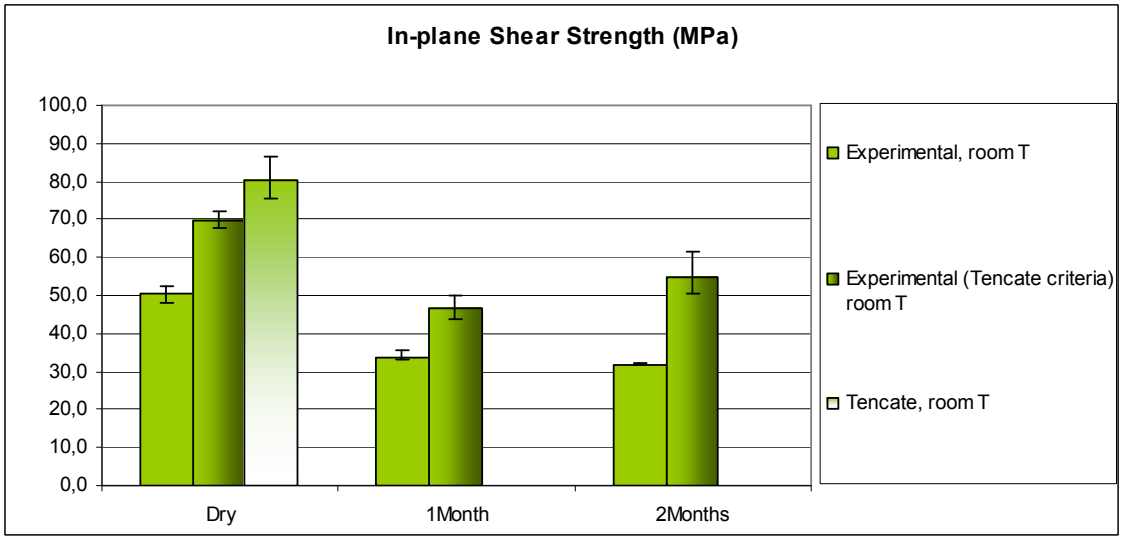

Fig.5.19 Change in in-plane shear strength with time of conditioning for GF/PPS.

Again, as the in-plane shear test is a matrix and interface dominant behaviour test the same conclusion was found as for the flexural test. A remarkable retention of properties in CF/PPS versus an important loss of properties of GF/PPS, with a loss of 40% for modulus and 37% for in-plane shear strength.

The tested in-plane shear specimens, for all conditions of ageing are shown in Fig.5.20. Please note the change in the use of paper tabs explained in Appendix 5.

Fig. 5.20 In-plane shear tested specimens.

5.5 SEM/EDS results

In this section the conclusions from the micro-scale analysis are given.

Two of the EDS spectra obtained during testing and the species found on the scanned surface are depicted in Fig.5.21 and Fig.5.22 for CF/PPS and GF/PPS. The spectra varied with the analyzed area (matrix or fibers, inside the composite or on the surface) and the water content (dry or saturated). Table 5.4 and Table 5.6 show the corresponding counting of elements. The counting could be restricted to the elements to study, e.g. reduced counting for the same saturated CF/PPS matrix area is shown in Table 5.5.

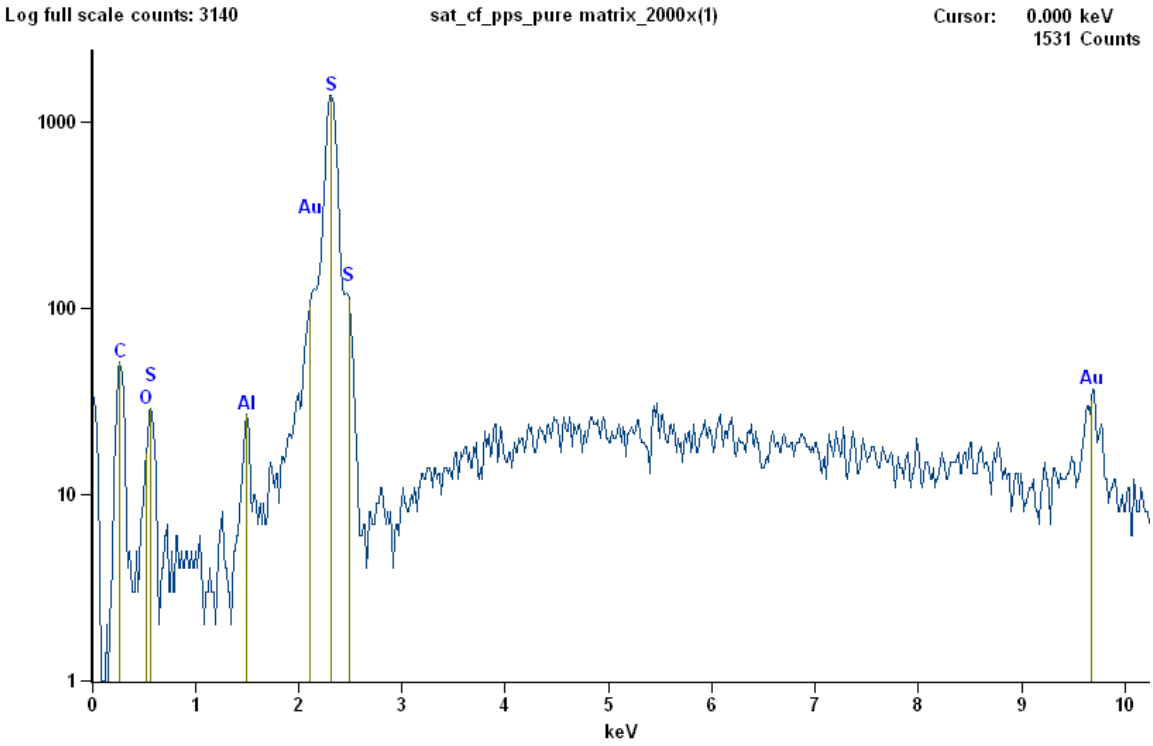

Fig.5.21 Spectra of saturated CF/PPS matrix area.

Table 5.4 Counting of elements of the above saturated CF/PPS matrix area spectra.

Element Line	Net Counts	Net Counts Error		Weight %	Weight % Error	Atom %	Atom % Error
C K	437	+/-	18	22.64	+/- 0.93	57.94	+/- 2.39
O K	225	+/-	29	2.57	+/- 0.33	4.94	+/- 0.64
Al K	180	+/-	17	0.21	+/- 0.02	0.23	+/- 0.02
S K	16992	+/-	215	31.45	+/- 0.40	30.15	+/- 0.38
S L	0		0	---	---	---	---
Au L	600	+/-	78	43.14	+/- 5.61	6.73	+/- 0.88
Au M	1628	+/-	135	---	---	---	---
Total				100.00		100.00	

Table 5.5 Restricted counting to the elements to study of the above saturated CF/PPS matrix area spectra.

Element Line	Net Counts	Net Counts Error		Weight %	Weight % Error	Atom %	Atom % Error
C K	446	+/-	27	53.92	+/- 3.26	73.31	+/- 4.44
O K	228	+/-	30	6.30	+/- 0.83	6.43	+/- 0.85
S K	15881	+/-	193	39.78	+/- 0.48	20.26	+/- 0.25
S L	0		0	---	---	---	---
Total				100.00		100.00	

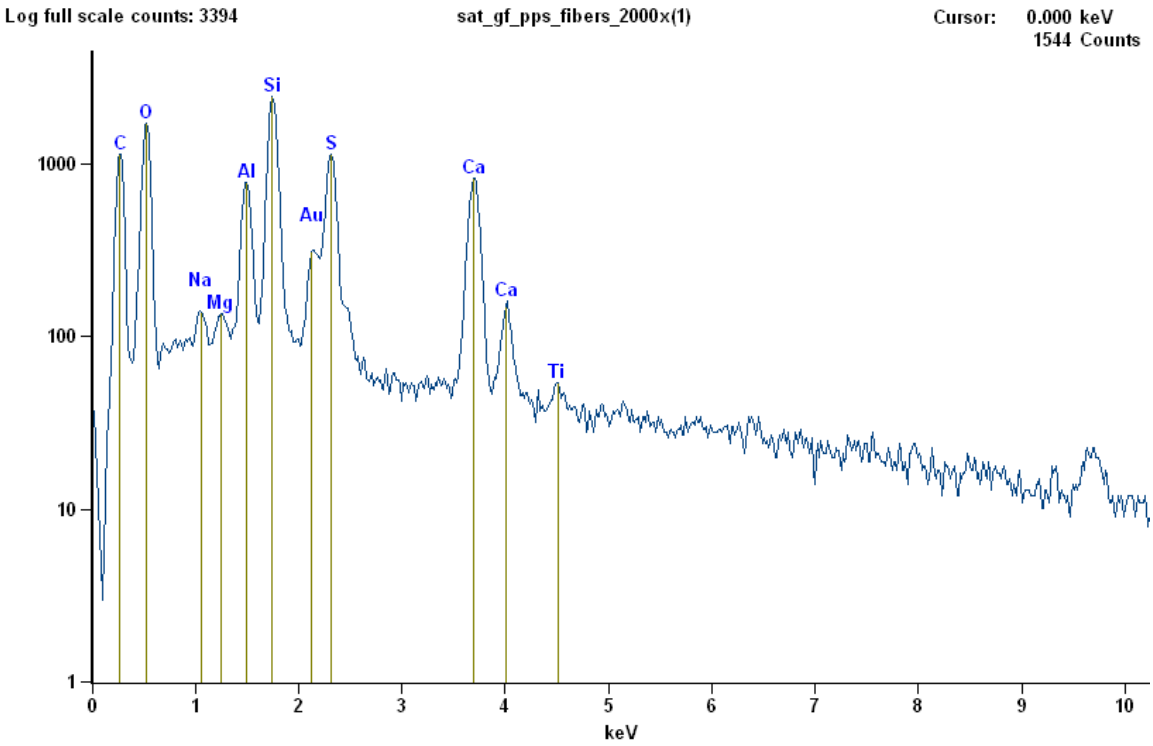

Fig.5.22 Spectra of saturated GF/PPS fiber area.

Table 5.6 Counting of elements of the above saturated GF/PPS fiber area spectra.

Element Line	Net Counts	Net Counts Error	Weight %	Weight % Error	Atom %	Atom % Error
C K	9183	+/- 122	44.92	+/- 0.60	60.20	+/- 0.80
O K	13732	+/- 169	29.20	+/- 0.36	29.38	+/- 0.36
Na K	470	+/- 51	0.25	+/- 0.03	0.17	+/- 0.02
Mg K	431	+/- 61	0.12	+/- 0.02	0.08	+/- 0.01
Al K	6985	+/- 99	1.94	+/- 0.03	1.16	+/- 0.02
Si K	23964	+/- 252	6.44	+/- 0.07	3.69	+/- 0.04
S K	12779	+/- 271	4.81	+/- 0.10	2.42	+/- 0.05
S L	0	+/- 15	---	---	---	---
Ca K	10655	+/- 187	5.76	+/- 0.10	2.31	+/- 0.04
Ca L	0	+/- 74	---	---	---	---
Ti K	212	+/- 47	0.17	+/- 0.04	0.06	+/- 0.01
Ti L	0	+/- 50	---	---	---	---
Au L	284	+/- 73	6.38	+/- 1.64	0.52	+/- 0.13
Au M	4488	+/- 219	---	---	---	---
Total			100.00		100.00	

In the case of CF/PPS this technique proved to be very useful to locate water content. Oxygen has to be found to denote the content of water, since hydrogen is not detected with this technique. As the CF and PPS do not contain oxygen, the presence of oxygen can be used to indicate water. When pure carbon fibers were analyzed, no oxygen was found, so the carbon fibers remained basically dry. The more sulphur found, the more oxygen was counted. As PPS is hydrophobic, it can be said that this oxygen is found at the interface. As the content of water was so low, the amount of oxygen found from dry matrix to saturated matrix, was comparable.

Some accidental traces of other chemical elements were found by the EDS method: gold (Au) and aluminium (Al). The presence of Au was due to the applied superficial treatment of the samples. A more interesting result is the presence of Al.

In the case of CF/PPS, Al was not found in the dry material but it was in the saturated one. It seemed that the specimens were contaminated in the climate chamber. This accidental phenomenon could be used in future research to trace and map the humidity content.

In the case of GF/PPS it was more complicated to monitor the humidity uptake by EDS due to the fact that the oxygen in the oxides of the GF are mixed in the counting with the oxygen of water. However, a more relevant result and a clue for the conclusions of this research was the presence of different types of cations, e.g. Na^{+}, Mg^{+2}, Si^{+4}, Ca^{+2}, Ti^{+4} (see Table 5.6 and Table 2.3), partially belonging to the GF and partially belonging to the sizing of the GF. The polar nature of these elements indicates the more sensitivity of the GF/PPS composites to water as explained in section 2.7 Glass fibers. Most probable, these polar components are reacting with water, taking up more water easily than in the case of CF/PPS, where carbon is apolar. These combinations between water and the GF components weaken the interface. This is revealed in the significant loss of matrix and interface dominant properties, shown in the section 4.7 Mechanical testing.

The micrographs show a good homogeneity of the composite in both dry composites (CF and GF/PPS). The dry material appeared to be void-less. This fact is supported by the good results in C-scan explained previously (see Fig.5.23 and Fig.5.24). The different distribution of fibers in the matrix in both systems can be seen, more disperse in CF/PPS and more concentrated in GF/PPS.

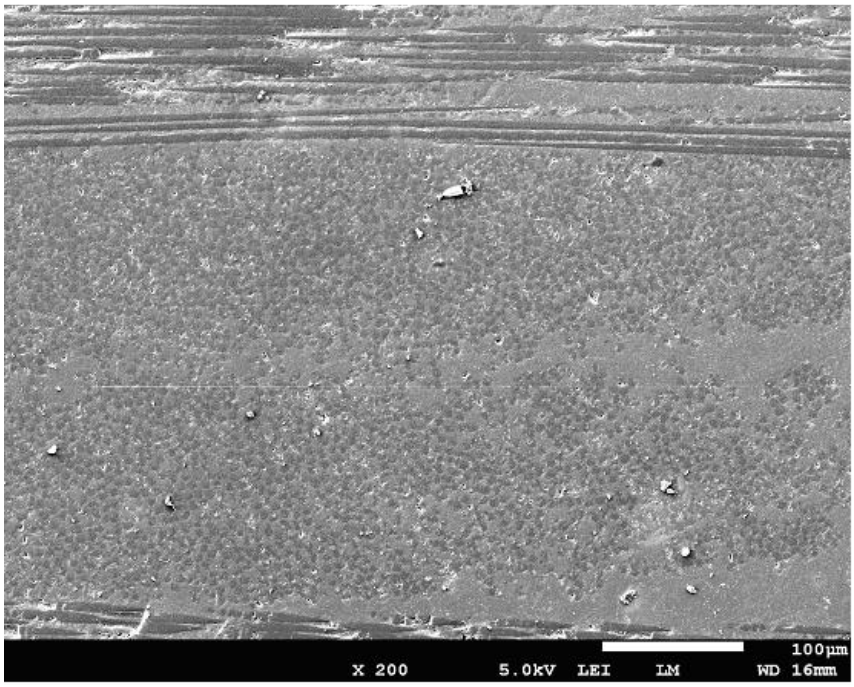

Fig.5.23 Dry CF/PPS(x200).

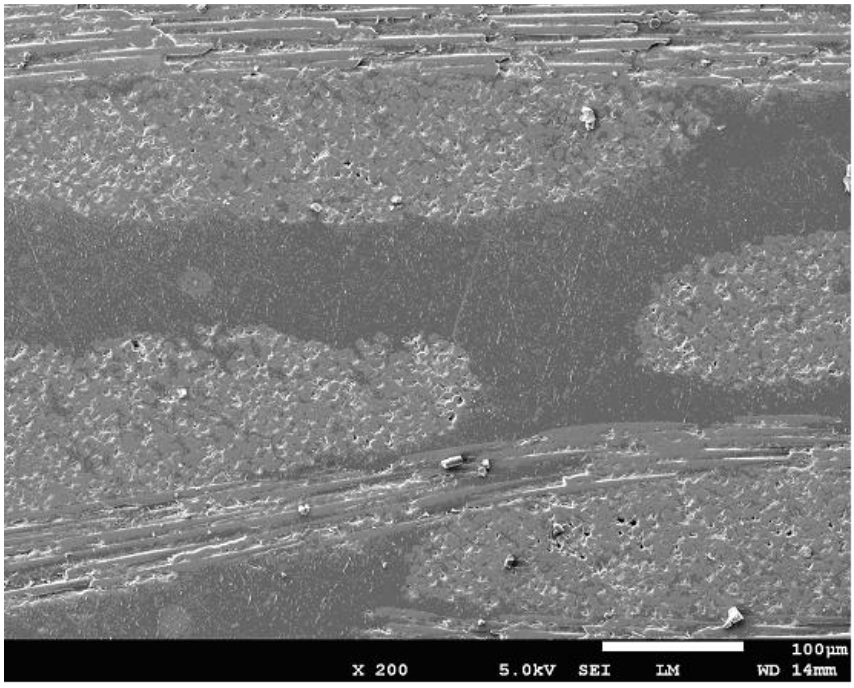

Fig.5.24 Dry GF/PPS(x200).

A higher magnification of the dry material gives more insight in the results of this research; the different interfaces of CF versus GF (see Fig. 5.25 and Fig. 5.26). While CF present a rough surface, GF have a more regular smooth surface as explained in sections 2.6 Carbon fibers and 2.7 Glass fibers.

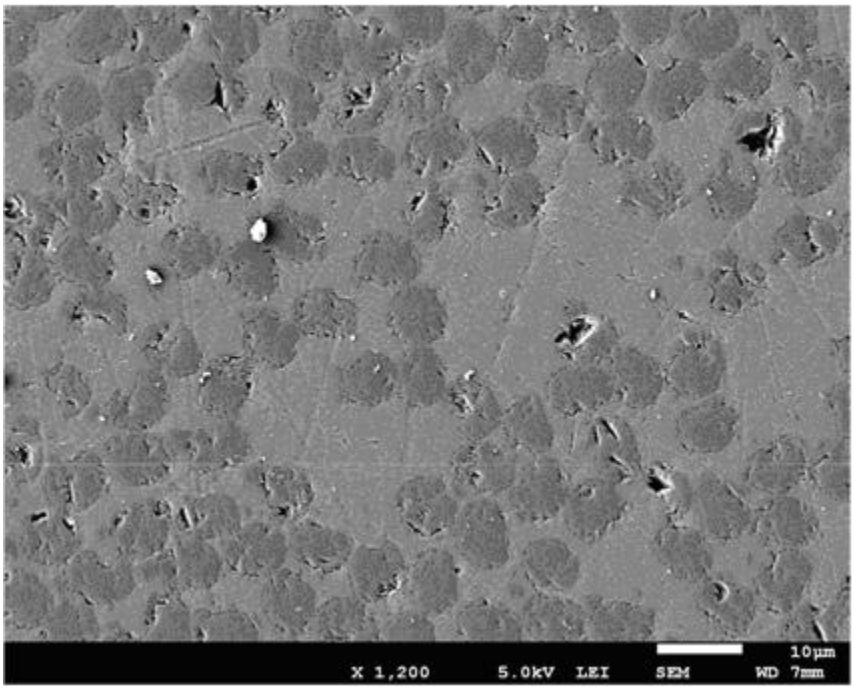

Fig.5.25 Carbon fiber(x1200).

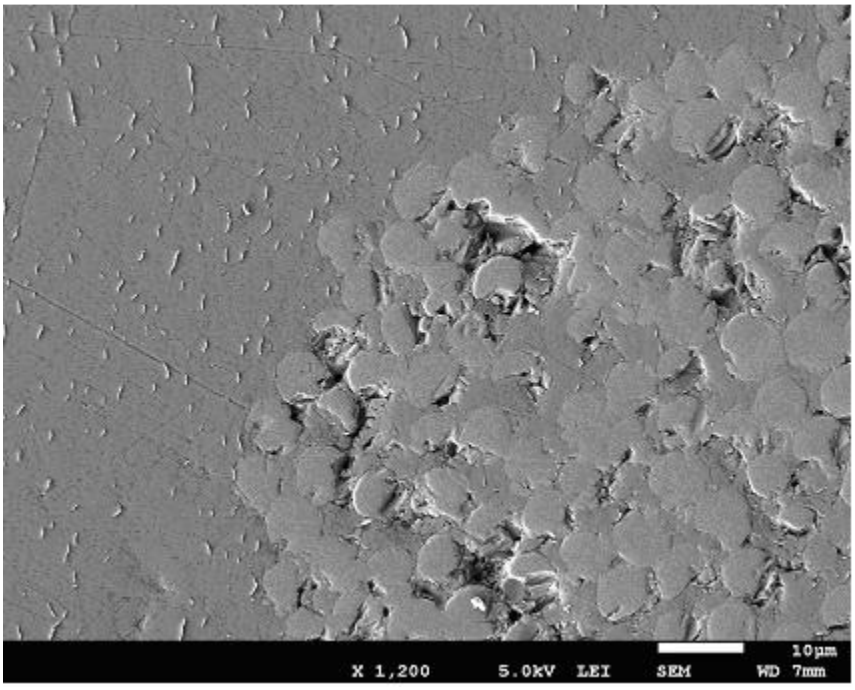

Fig.5.26 Glass fiber (x1200).

After conditioning no remarkable difference was found that could show an increase in the presence of cracks due to the moisture uptake. As the content of water is so low after saturation, micrographs did not clearly show the effect of humidity uptake when saturated material was scanned. Perhaps this also support the fact that water is affecting the chemical bond and is not damaging the material through cracks as the diffusion of water is so low. In both saturated CF and GF tensile tested material no significance difference was found between dry and saturated systems.

More results were found in in-plane shear test of dry and saturated GF/PPS, as it is a matrix and interface dominant test, where the loss of properties raised to a 30%.

In Fig.5.27 and Fig.5.28 the smooth surface of the GF after failure in dry GF/PPS can be seen. Fibers within the fiber bundles get detached from the resin which is favoured in the case of saturated GF/PPS (see Fig. 5.29 and Fig.5.30) due to the weakening of the interface by the water action.

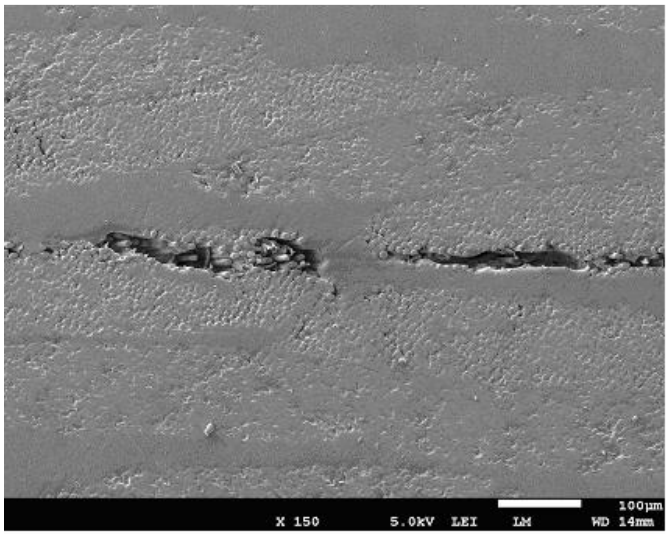

Fig.5.27 Dry in-plane shear tested GF/PPS(x150).

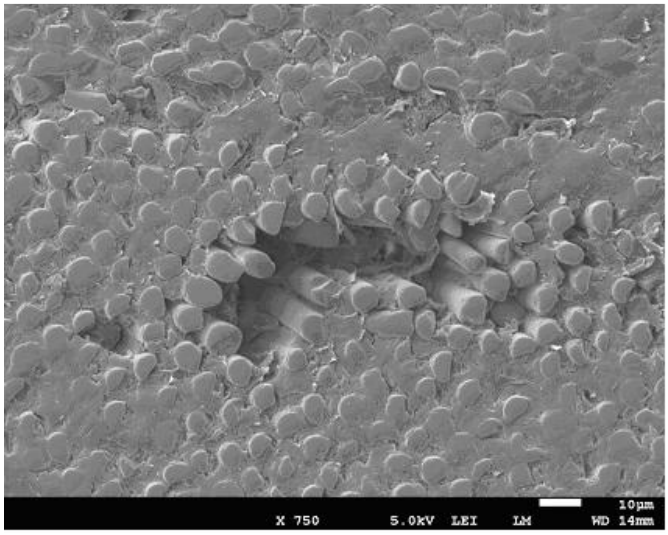

Fig.5.28 Dry in-plane shear tested GF/PPS(x750).

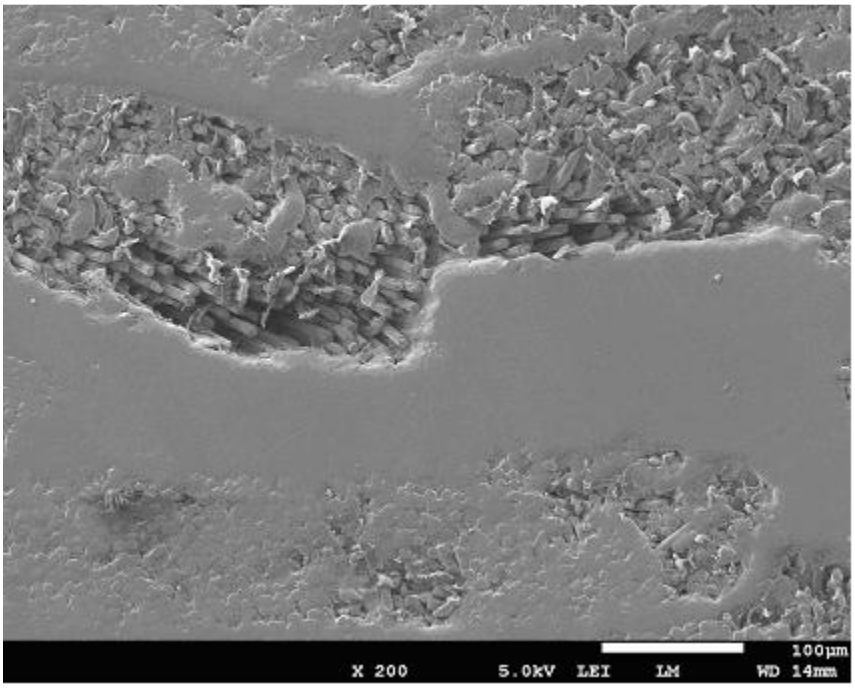

Fig.5.29 Saturated in-plane shear tested GF/PPS(x200).

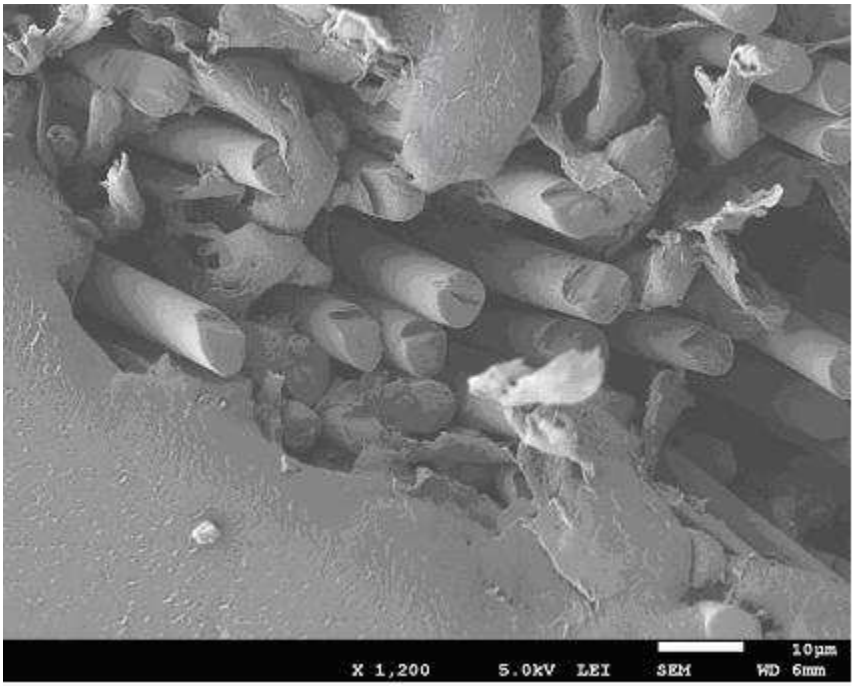

Fig.5.30 Saturated GF/PPS in-plane shear (x1200).

In order to show a better resistance against water ingress of CF/PPS interface, saturated CF/PPS in-plane shear tested material was also researched and is shown in Fig.5.31. It can be noticed that even for the saturated CF/PPS, the interface in the failure zone remained intact.

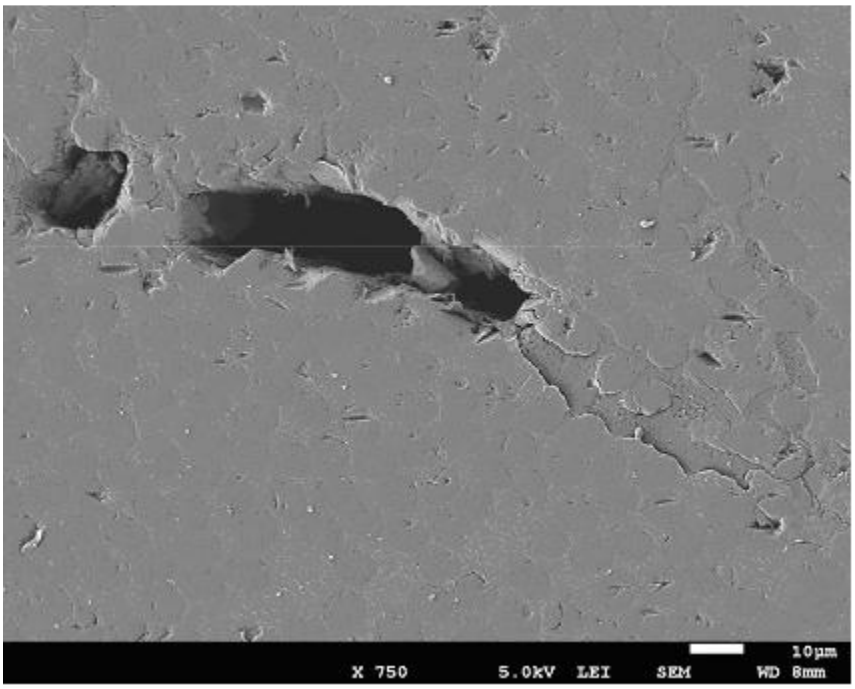

Fig.5.31 Saturated in-plane shear tested CF/PPS (x750).

Also tensile tested material was inspected. Dry, saturated, 120ºC and saturated-120°C tensile tested material were analysed but no differences could be found between them.

CHAPTER 6: CONCLUSIONS AND RECOMMENDATIONS

PPS composites absorb low levels of humidity; 0.17% for CF/PPS and 0.21% for GF/PPS, in this research, at 80ºC and 90%RH after 2 months of conditioning.

The diffusion of the water in the composite can be modelled assuming Fick's diffusion law. Diffusion coefficients of 0.005 and 0.010 mm^2/h were derived for CF/PPS and for GF/PPS respectively. A rather high variation coefficient, 35% and 37%, was found though. Some recommendations that could be followed to improve the repeatability of the diffusion coefficients are suggested below:

4. Bigger specimens or sealed edge specimens shall be used to follow procedure A of the ASTM D5229, especially in very low humidity uptake saturation levels, like those found in this research (0.21%, 0.17%).
5. More measurements in the first 72 hours are needed for the linear part of the Fick's law. This part of the model can extend to this short initial period.
6. A weighing method error of ±10 mg is recommended to be used to round off weights of specimens.

CF/PPS presented a significant retention of mechanical properties even after saturation and at tensile testing temperatures above Tg (120°C).

GF/PPS was sensitive to humidity uptake when tested under matrix and interface dominant tests like in-plane shear and three point bending. Losses up to 30% of mechanical properties were calculated after saturation in the mentioned tests.

SEM/EDS technique came up to be useful to find humidity uptake in the case of CF/PPS since no oxygen is present in the dry system. On the other hand, the presence of oxygen in the oxides of the GF made this technique non-applicable in this case.

An accidental contamination of Al in the climate chamber arose as a possible method for tracing in future humidity uptake researches.

Although no direct measure for the water in the GF/PPS samples was possible, the EDS technique was useful to find the chemical elements present in the GF. Different cations were found, part of them belonging to the fiber itself, and the rest to the sizing (the superficial treatment). The polar nature of these elements is assigned as one of the reason of the sensitivity of the GF system to humidity uptake. The coupling of these elements with water seems to explain the weakening of the interface.

This hypothesis was supported by the micrographs that showed a detachment of the GF and the matrix in saturated tested specimens.

The roughness of the CF versus the smoothness of the GF could also explain the more difference in interface behaviour.

The influence of testing temperature, where a decrease in properties was found both for CF/PPS and GF/PPS, is explained by the presence of a glass transition temperature (Tg) of thermoplastics. The softening of the matrix above Tg could explain the decrease in tensile properties. Matrix dominant tests should be performed to show this effect even more.

While the effect of temperature damage can be observed almost instantaneously, a similar loss in properties was observed after humidity uptake after 2 months.

Other variables that could be monitored in future similar researches could be:

- The quantified water absorption by other techniques, different from a gravimetric method, like infrared spectroscopy.
- The effect of thickness, percentage of fibers, degree of crystallinity or glass transition temperature on diffusion coefficient and humidity saturation measurements.
- The influence of fiber content, the evolution of glass transition temperature and crystallinity during conditioning on the mechanical properties.
- The effect of the surface treatment of the fibers on mechanical properties and the behaviour of the sizing with humidity uptake.

LIST OF REFERENCES

1.1 http://www.ides.com/supplierportal/solvay.asp

2.1 Ageing of composites, Edited by Rod Martin , 1st edit, Woodhead Publishing and Maney Publishing on behalf of The Institute of Materials, Minerals & Mining, Cambridge, England, 2008.

2.2 http://www.azom.com/article.aspx?ArticleID=83

2.3 Hygrothermal Effects in Continous Fibre Reinforced Composites. Part I: Thermal and Moisture Diffusion in Composite Materials, J.P. Komorowski, National Aeronautical Establishment, Ottawa, January, 1993.

2.4 Environmental Effects on the Water Absorption and Mechanical Properties of Carbon Fiber Reinforced PPS and PEEK Composites. Part II, Chen-chi M. Ma *and* Shih-Wen Yur, Institute of Chemical Engineering, National Tsing Hua University Hsin-Chu, Taiwan, 30043, Republic of China, Polymer Engeneering and Science, Mid-January 1991, Vol. 31, No. 1.

2.5 ASTM D5229/D5229M-92 (Reapproved 2004) Standard Test Method for Moisture Absorption Properties and Equilibrium Conditioning of Polymer Matrix Composite Materials, Published March, 2004, United States.

2.6 http://chem.chem.rochester.edu/~chem424/pps.htm

2.7 Hygrothermal Effect on the Mechanical Properties of Polyphenylene Sulfide (PPS) Composites, Jirui Chen, Department of Mechanical Engineering at Concordia University, Montreal, Quebec, Canada, May, 1990.

2.8 http://www.compositesworld.com/articles/the-making-of-carbon-fiber

Article From: High-Performance Composites January2009, Vicki McConnell

Posted on: 19/12/2008

2.9 http://www.compositesworld.com/articles/the-making-of-glass-fiber

Article From: Composites Technology April 2009, Ginger Gardiner

Posted on: 25/3/2009

2.10 http://www.compositesworld.com/articles/sizing-up-fiber-sizings

Article From: Composites Technology April 2006, Karen Mason

Posted on: 1/4/2006

3.1http://www.tencate.com/TenCate/Aerospace_composites/documents/TCAC%20USA%20docs/TCAC%20USA%20Datasheets/DataSheet/DS%20PPS%20CETEX%20WEB.pdf

4.1 ASTM D3518/D 3518M – 94 (Reapproved 2001) Standard Test Method for In-Plane Shear Response of Polymer Matrix Composite Materials by Tensile Test of a ±45° Laminate, Published January, 1995, United States.

4.2 ASTM D3039/D3039M – 00 (Reapproved 2006) Standard Test Method for Tensile Properties of Polymer Matrix Composite Materials, Published January, 2008, United States.

4.3 ASTM D7264/D7264M – 07 Standard Test Method for Flexural Properties of Polymer Matrix Composite Materials, Published April, 2007, United States.

5.1 Personal communication with Serge van Meer, responsible technician for C-scan (28-10-2010).

APPENDIX 1: GEOMETRY AND SAMPLING OF HUMIDITY UPTAKE SPECIMENS

For the humidity uptake, the geometry of the specimens recommended in ASTM D5229 (Ref.2.5) is summarized in Table app.1.2 (Ref.2.5). Dimensions are related also to the balance accuracy requirement shown in Table app.1.1 (Ref.2.5).

Table app.1.1. Appropiate accuracy of analytical balance and specimen mass *(Ref. 2.5).*

Specimen Mass, g	Balance Accuracy Requirement, mg
≥5 but <50	0.1
≥50	1.0

The specimen thickness, derived from the 8 layers of the stacking, was fixed. The diffusion coefficients were unknown. Non-sealed edges bare specimens were chosen, neglecting side effects of the humidity uptake. The fact that the specimens used to measure Fick's diffusion properties will be used after conditioning to test the tensile properties in hot temperatures forced the decision of rectangular shape according to the ASTM D3039 (Ref.4.2), (see Table app.1.2).

Table app.1.2 Summary of humidity uptake specimen geometry requirements (Ref. 2.5 and Ref.4.2).

	Known Specimen Thickness (mm.)	1. Determine the reference time period from 10.1.7.1(Ref.2.5). If the value so determined is unacceptable then the specimen thickness must be changed.	2. Determine the plate size from either Eq 2 (non-sealed edges) or 8.2.4.2 (sealed edges) (Ref.2.5).	3.W(mm) of a nominally square plate or curved panel	4.Specimens must be tested under tensile load ⇩ (Ref.4.2) Rectangular shape with Width=25 mm And length (mm):
CF/PPS	2.38	Unknown D_z ⇩ Reference time period=7 days ⇩ Acceptable	Non-sealed edges ⇩ (w/h)≥100 w = nominal length of one side of a nominally square plate or curved panel, (mm) h = nominal thickness, (mm)	≥238	≥250
GF/PPS	1.89			≥189	≥250

Therefore, a length of 28 cm. was chosen to simplify the cutting. Since the mass of the specimens was below 50g, the balance accuracy (Ag204 of Mettler Toledo), see Fig. app.1.1, should be 0.1 mg. The final mass of the specimens was calculated from the data of specific gravity supplied by Tencate (Ref.3.1), shown in Table app.1.3 and the balance accuracy requirement is also included (Ref 2.5).

Table app.1.3 Recommended balance accuracy for the calculated specimen mass (Ref.2.5 and Ref.3.1).

	Specific gravity (SG) [g/cm³] (Ref.3.1)	Mass of the specimens(m) [g] m=SG*l*w*h l-length[cm] w-width[cm] h-thickness[cm]	Balance accuracy requirement [mg] (Ref 2.5)
T300 3K 5HS/PPS with double sided Amcor foil (CF/PPS)	1.55	m=1.55*28*2.5*0.238 m=25.82 g	0.1
7781/PPS (GF/PPS)	1.92	m=1.92*28*2.5*0.189 m=25.40 g	

Fig. app.1.1 Analytical balance.

Five specimens per material were cut and subsequently weighed as recommended in the corresponding standard.

APPENDIX 2: GEOMETRY AND SAMPLING OF TENSILE SPECIMENS

Tensile specimen geometry and sampling were planned according to the recommendations of the ASTM D3039 (Ref.4.2). Table app.2.1 shows the geometry recommendations.

Table app.2.1 Tensile specimen geometry recommendations (Ref.4.2).

Fiber Orientation	Width, mm	Overall Length, mm	Thickness, mm
balanced and symmetric	25	250	2.5

The CF/PPS laminate thickness was close to the recommended one. The GF/PPS laminate thickness was less (1.89 mm) but as the decision of the 8 layers, and consequently, the thickness, was already fixed as explained previously, this recommendation was ignored.

Five specimens were cut to be tested after each condition of ageing and for each testing temperature.

APPENDIX 3: ESTIMATION OF TENSILE PROPERTIES AND APPARATUS SELECTION

A first calculation had to be done to choose the tensile bench to use. The expected UTS can be estimated from the data of the UTS by Tencate (Ref.3.1) and the maximum load derived, known the geometry of the coupons (see Table app.3.1, Ref.3.1 and Ref.4.2).

Table app.3.1 Estimation of the maximum load (Ref.3.1 and Ref.4.2).

	Ultimate tensile strength (UTS) (23°c/50%RH) (Ref.3.1) [MPa]	Cross section (s) [mm^2]	Maximum Load[KN] =UTS[MPa]*s[mm^2] *10^{-3} (Ref.4.2)
T300 3K 5HS/PPS with double sided Amcor foil (CF/PPS)	758	59.35	45
7781/PPS (GF/PPS)	340	47.25	16

The available tensile machines were Zwick 20KN, and Zwick 250 KN of Zwick Roell Group. Thus the procedure of testing tensile properties was undertaken in the Zwick 250 KN testing machine.

APPENDIX 4: GEOMETRY AND SAMPLING OF IN-PLANE SHEAR SPECIMENS

The standard used to evaluate the in-plane shear properties was the ASTM D 3518 (Ref.4.1).
The recommended geometry shall be in accordance with ASTM D3039 (Ref.4.2) The next consideration has to be followed; the stacking sequence shall be [45/−45]*ns*, with 2<n<4 for woven fabric (8,12 or 16 plies). As explained above, the thickness is given by the thickness of 8 layers. Also it has to be notice that the laminate had to be cut in the diagonal to get the [45,-45]º orientation of the fibers, see Fig. app.4.1 (Ref. 4.1), as the stacking was performed with a [0,90]º orientation.

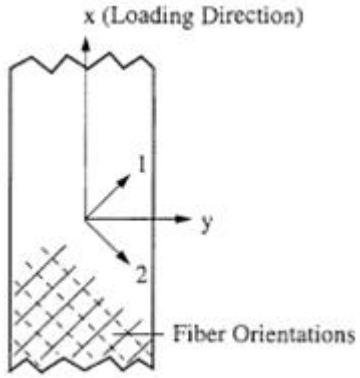

Fig. app.4.1 Definition of Specimen and Material axes. "x" and "y" represent the Specimen or Reference axis, while 1 and 2 represent the Material or Local Axes (Ref.4.1).

The recommended coupon width is 25 mm, and the length range is 200 to 300 mm. A length of 250 mm was chosen. The sampling shall be in accordance with the ASTM D3039, therefore at least five specimens were tested for every condition.

APPENDIX 5: ESTIMATION OF IN-PLANE SHEAR PROPERTIES AND APPARATUS SELECTION

A first calculation had to be done to choose the tensile bench to use. The expected in-plane shear strength (IPSS) can be estimated from the data by Tencate (Ref.3.1) and the maximum load derived, known the geometry of the coupons (see Table app.5.1, Ref.3.1 and Ref.4.1).

Table app.5.1 Estimation of the maximum load in in-plane shear test (Ref.3.1 and Ref.4.1).

	In-plane shear strength (IPSS) (23°c/50%RH) (Ref.3.1) [MPa]	Cross section (s) [mm^2]	Maximum Load[KN] =IPSS[MPa]*2*s[mm^2] *10^{-3} (Ref.4.1)
T300 3K 5HS/PPS with double sided Amcor foil (CF/PPS)	119	59.35	14
7781/PPS (GF/PPS)	80	47.25	8

Then Zwick 20 KN could be used. Tabs are not required for this type of test, although at the start of testing, paper tabs were used. Detaching of paper tabs and slipping in the grips were observed in the case of CF/PPS material. Trying to test without paper tabs led to the same failure. Thus the tests were undertaken in the Zwick 250 KN with mechanical grips, which are different from those often used in the Zwick 20 KN (see Fig. app.5.1). Then the tests ran correctly.

Fig. app.5.1 Mechanical Grips often used in the 20KN Zwick.

APPENDIX 6: GEOMETRY AND SAMPLING OF THREE POINT BENDING SPECIMENS

The geometry is given in this case by the standard span-to-thickness ratio, which is 32:1 (Ref.4.3). With this span-to-thickness ratio it can be assured that failure occurs at the outer surface of the specimen, due only to the bending moment. The standard specimen width is 13 mm with the specimen length being about 20% longer than the support span. The dimensions used are explained in the Table app.6.1 (Ref. 4.3) below. The sampling again was at least 5 specimens per condition.

Table app.6.1 Geometry of three point bending specimens (Ref. 4.3).

	Thickness (t)[mm]	Span-to-thickness ratio (str)	Span(s)=t*str [mm]	Length(l)≥1.2*s [mm]	Width [mm]
CF/PPS	2.38	32:1	76.16	≥91.39	13
GF/PPS	1.89		60.48	≥72.58	

APPENDIX 7: ESTIMATION OF THREE POINT BENDING PROPERTIES AND APPARATUS SELECTION

Before initiating the test, the expected value of the maximum load was calculated from the data supplied by Ten Cate and the geometry of the specimens, see Table app.7.1 (Ref.3.1 and Ref.4.3).

Table app.7.1 Estimation of the maximum load in three point bending (*Ref.3.1 and Ref.4.3.)*

	Flexural strength warp (FSW) (23°c/50%RH) (Ref.3.1) [MPa]	Width (w) [mm]	Thickness (t) [mm]	Span (l) [mm]	Maximum Load[KN] =FSW[MPa]*2/3*w[mm]* (t[mm]) ^{2} /l[mm] *10^{-3} (Ref.4.3)
T300 3K 5HS/PPS with double sided Amcor foil (CF/PPS)	1027	13	2.38	76.16	0.7
7781/PPS (GF/PPS)	511		1.89	60.48	0.3

Therefore the Zwick 20KN testing machine was used.

APPENDIX 8: CALCULATION OF ERROR BY DESCRIPTIVE STATISTICS

One way to calculate the error of a direct measurement is to repeat the same measurement several times. If the same value is always obtained, the accuracy of the apparatus is not high enough to show the errors. When the measurement is repeated and different values appear, the accuracy of the instrument allows obtaining the errors in the measurement method.

In this case, the value of the measurement is the average and the error of the measuring method is the standard deviation (Ref.app.8.1).

A dry specimen kept in the desiccators was weighed weekly similar to the conditioned specimens. The results for both materials are shown in Table app.8.1.

Table app.8.1 Weight of a dry specimen kept in the desiccator.

	Average weight (mg)	Standard deviation (mg)	Measurement (mg)
CF/PPS	26595,5	2,8	26595±3
GF/PPS	26117,7	10,9	26120±10

If the same method is used to weigh a dry specimen of both materials, the error of the humidity uptake weighing method can be estimated with the bigger error, ±10 mg to round off every measurement.

App.8.1 BECKWITH, Thomas G. MARANGONI, Roy D. LINHARD V. John H. Mechanical measurements 2007 Pearson/Prentice Hall 6th ed. ISBN 0201847655